Research Square

Preprints are preliminary reports that have not undergone peer review.
They should not be considered conclusive, used to inform clinical practice,
or referenced by the media as validated information.

Mathematical Modeling of Co-Infection Dynamics of Malaria and Typhoid Fever with Control Measures

Philip Oladapo Olanrewaju
Federal University Wukari
Isaac Adesola Olopade
isaac.olopade@fuwukari.edu.ng

Federal University Wukari
Abdul Kareem Adamu
Federal University Wukari

Research Article

Keywords:

Posted Date: November 23rd, 2026

DOI: https://doi.org/10.21203/rs.3.rs-11801678/v1

License: This work is licensed under a Creative Commons Attribution 4.0 International License.
Read Full License

Additional Declarations: No competing interests reported.

Mathematical Modeling of Co-Infection Dynamics of Malaria and Typhoid Fever with Control Measures

Olanrewaju Philip Oladapo[1], Olopade, Isaac Adesola[2] and Adamu Abdul Kareem[3]

[1,2,3]Department of Mathematics, Federal University Wukari, PMB 1020, Wukari, Taraba State, Nigeria

Corresponding Author: isaac.olopade@fuwukari.edu.ng

Abstract

Co-infection with malaria and typhoid fever poses a major public health challenge, especially in tropical regions. This study develops a mathematical model to analyze the co-infection dynamics, incorporating environmental sanitation and treatment interventions. The model uses differential equations to represent human populations in various disease states and derives the basic reproduction number (R_0) to assess disease persistence or eradication.

Stability analysis shows that when $(R_0 < 1)$, the disease-free equilibrium is stable, indicating eradication, while $(R_0 > 1)$ leads to a stable endemic equilibrium, signifying persistent co-infection. Sensitivity analysis identifies key parameters influencing (R_0) and numerical simulations reveal that combining environmental sanitation and treatment significantly reduces co-infection prevalence. The study provides insights for public health strategies by highlighting the effectiveness of integrated interventions in controlling both malaria and typhoid fever.

1. Introduction

Co-Infection of Malaria and Typhoid

Co-infection involves simultaneous infection by multiple pathogens, often occurring in low-resource, high-disease-burden regions with poor sanitation, overcrowding, and tropical climates [1]. These infections complicate diagnosis and treatment, as overlapping symptoms and immune interactions may worsen disease outcomes [2].

A notable example is the co-infection of malaria and typhoid fever, common in Sub-Saharan Africa and South Asia where conditions favor both mosquito proliferation and fecal-oral transmission [1, 3, 4. Malaria remains a major public health challenge, particularly in Africa, where *Plasmodium falciparum* is the predominant causative parasite and transmission occurs primarily through the bites of infected *Anopheles* mosquitoes. Despite significant advances in vector control, improved case management, and chemoprevention, the disease continues to account for considerable morbidity and mortality [20, 21]. Similarly, typhoid fever, caused by *Salmonella enterica*serovar Typhi, persists as an important health burden in many developing settings. Its continued transmission is largely associated with inadequate sanitation, unsafe water supplies, and poor hygiene practices, which promote the faeco-oral spread of the infection [19, 22, 23].

Malaria and typhoid fever, together challenge the immune system, malaria-induced anemia increases susceptibility to bacterial infections, while typhoid-related inflammation can aggravate malaria symptoms [5, 7]. Such co-infections heighten morbidity, mortality, and healthcare burdens [3, 19, 20].

Diagnosing malaria-typhoid co-infection is particularly difficult due to symptom overlap, limited diagnostic tools, and weak health infrastructure [3, 26, 27]. Studies show that up to 20% of febrile patients in endemic areas suffer from both infections [7, 28]. This contributes to extended recovery, misdiagnosis, and increased treatment costs.

Malaria alone accounts for 249 million global cases as of 2023, with over 90% in Sub-Saharan Africa [3]. It spreads via bites from infected Anopheles mosquitoes, causing cyclical fevers and complications like cerebral malaria if untreated [3, 8]. Control efforts face challenges from insecticide resistance and poor infrastructure [9]. Effective management depends on prompt diagnosis, parasite identification, and appropriate treatment [3, 15].

Typhoid fever, caused by S. Typhi, spreads through contaminated food and water. Some of its symptoms are; fever, abdominal pain, and fatigue, which can progress to intestinal or neurological complications if untreated [6]. The disease is prevalent in regions lacking sanitation, and asymptomatic carriers can facilitate its spread [4, 5]. Early antibiotic treatment, along with access to clean water, is vital for control [4].

The dual burden of these diseases is worsened by diagnostic confusion, delayed treatment, and compounding effects on immunity, despite their public health importance.

Mathematical modelling has emerged as a valuable framework for investigating the spread and progression of infectious diseases, estimating key epidemiological thresholds, assessing the potential impact of intervention measures, and supporting evidence-based public health decision-making. A wide range of compartmental models have been developed to describe malaria transmission, incorporating important factors such as vector–host interactions, acquired immunity, vaccination, imported cases, seasonal variation, and treatment or other control measures [18, 20, 29–34]. Similarly, mathematical models of typhoid fever have explored the roles of environmental contamination, chronic carriers, treatment, relapse, vaccination, and hygiene-related interventions in shaping disease transmission and persistence [25, 34–39]. Collectively, these modelling studies have enhanced understanding of the distinct transmission processes and epidemiological factors underlying malaria and typhoid fever.

Relatively limited attention has been given to the mathematical investigation of the joint transmission dynamics of malaria and typhoid fever. Among the available studies on malaria–typhoid co-infection, the deterministic model proposed by [40] represents one of the notable and widely referenced contributions. Nevertheless, since the development of such early models, infectious disease modelling has evolved considerably, with increasing applications of bifurcation analysis, uncertainty quantification, local and global sensitivity analysis, and more detailed representations of disease progression.

[12] Incorporated drug-resistant malaria, optimal control, and cost-effectiveness analysis into a malaria–typhoid co-infection model. Their numerical results highlighted the potential benefits of controlling drug-resistant malaria and targeting typhoid sources and carriers. Nevertheless, the generalizability of their recommendations depends on the reliability of the parameter values and economic assumptions employed.

[10] Developed a deterministic model incorporating mosquito-mediated malaria transmission and loss of immunity. Using reproduction thresholds and equilibrium stability analysis, the authors investigated conditions governing disease persistence and elimination. Their work extended existing models by accounting for waning immunity, although further empirical validation could strengthen its practical applicability.

[13] examined typhoid co-infection with Plasmodium vivax and Plasmodium falciparum, incorporating treatment into the model. Their analysis included equilibrium solutions, reproduction numbers, stability, sensitivity analysis, and numerical simulations. By distinguishing between malaria parasite species, the study broadened the modelling framework, although setting-specific calibration remains important for reliable predictions.

[11] Developed a model incorporating human infection compartments, temporary immunity, mosquito transmission, and environmental bacterial contamination. Their study examined reproduction thresholds, equilibrium stability, sensitivity, and control strategies, and fitted the model to Nigerian malaria data. However, the absence of corresponding long-term typhoid incidence data limited the empirical calibration of the typhoid component.

Despite advances in malaria–typhoid co-infection modelling, limited attention has been given to the combined effects of human, vector, and environmental factors on disease persistence and control. In particular, the roles of environmental sanitation and Salmonella Typhi concentration in contaminated water in influencing typhoid transmission remain insufficiently explored. To address these gaps, this study develops a deterministic mathematical model, building on [10] that incorporates environmental sanitation, bacterial concentration and disinfection efforts to investigate malaria–typhoid co-infection dynamics and identify key parameters influencing disease persistence. The model also considers treatment of either or both infections in co-infected individuals and assumes temporary immunity following recovery. The findings are expected to inform integrated control strategies for malaria and typhoid fever in endemic regions.

2.0. Deterministic Model Formulation and Description

A deterministic compartmental model is developed to study the co-infection dynamics of malaria and typhoid fever, incorporating three interacting populations: the human population, the vector population (mosquitoes), and the bacterial population (Salmonella Typhi concentration). The human population is subdivided into ten distinct compartments: susceptible individuals (S), individuals exposed to malaria (E_M), individuals exposed to typhoid (E_T), individuals exposed

to both malaria and typhoid (E_{MT}), individuals infected with malaria (I_M), individuals infected with typhoid (I_T), individuals co-infected with both malaria and typhoid (I_{MT}), individuals recovered from malaria (R_M), individuals recovered from typhoid (R_T), and individuals recovered from co-infection (R_{MT}).The vector population is divided into two compartments: susceptible vectors (S_V) and infected vectors (I_V). The bacterial population is represented by a single compartment denoting the concentration of Salmonella Typhi in the environment (C). Altogether, this yields a comprehensive thirteen-compartment model, as described in (4). The total human population, (N) at time t becomes;

$$N_H(t) = S(t) + E_M(t) + E_T(t) + E_{MT}(t) + I_M(t) + I_T(t) + I_{MT}(t) + R_M(t) + R_T(t) + R_{MT}(t) \quad (1)$$

The total population of the vector is given by;

$$N_V(t) = S_V(t) + I_V(t) \quad (2)$$

While the concentration of Salmonella Typhi in the environment is given by;

$$C(t) \quad (3)$$

The flow of interaction and transition dynamics of the co-infection between the compartments is illustrated in figure 1. The definitions and biological interpretations of the state variables are provided in Table 1, while the corresponding model parameters, together with their descriptions and assigned values, are summarized in Table 2.Hence;

Table 1: Description of state Variables of the model

State Variable	Epidemiological Description
S	Susceptible Individuals
E_M	Exposed Malaria Individuals
E_T	Exposed Typhoid Individuals
E_{MT}	Exposed Malaria-Typhoid Individuals
I_M	InfectedMalaria Individuals
I_T	Infected Typhoid Individuals
I_{MT}	InfectedMalaria-Typhoid Individuals
R_M	Recovered Malaria Individuals
R_T	Recovered Typhoid Individuals
R_{MT}	Recovered Malaria-Typhoid Individuals
S_V	Susceptible Vectors
I_V	Infected Vectors
C	Concentration of Bacteria in the Environment

Table 2: Description and Parameter values of the model.

Parameter	Descriptions	Value	Source
Λ	Recruitment into susceptible compartment	750	[12]
α	Environmental sanitation	0.5	Assumed
β_1	Transmission rate of malaria by mosquito	2.8	[12]
β_2	Transmission rate of typhoid by humans	1.0125	[12]
β_3	Transmission rate of malaria/typhoid by humans	0.31	Assumed
β_V	Transmission rate of malaria by humans	0.3	[12]
ω_M	Waning rate of humans from recovered malaria in to susceptible	0.05	[14]
ω_T	Waning rate of humans from recovered typhoid into susceptible	0.0019	[14]
ω_{MT}	Waning rate of humans from recovered malaria/typhoid into susceptible	0.9	Assumed
a	Biting rate of mosquito	1.1	[12]
b	Number of humans bitten by mosquito per unit time	12	[14]
k	Exposure to the bacteria concentration	0.4	Assumed
μ_H	Natural death of human	0.0189	[12]
μ_V	Natural death of mosquito	0.1429	[12]
μ_C	Decay rate of bacteria concentration	0.0345	[12]
θ	Disinfectant of bacterial concentration	0.5	Assumed
σ_M	Progression from the exposed to infectious human malaria	0.2	[14]
σ_T	Progression from the exposed to infectious human typhoid	0.18	[14]

σ_{MT}	Progression from the exposed to infectious human malaria/typhoid	0.21	Assumed
γ_M	Treatment rate of infected malaria human	0.25	Assumed
γ_T	Treatment rate of infected typhoid human	0.20	Assumed
γ_{MT}	Treatment rate of infected malaria/typhoid human	0.32	Assumed
δ_{IM}	Disease induce death of malaria human	0.00228	[12]
δ_{IT}	Disease induce death of typhoid human	0.0024	[12]
δ_{IMT}	Disease induce death of malaria/typhoid human	0.03	Assumed
ρ_T	Shedding of disease into the bacteria concentration	10	[14]
π	Recruitment of mosquito into susceptible vector	600	[12]
ϕ_V	Mosquito death due to the spraying of insecticide	0.3	Assumed
N_H	Total population of human	10000	Assumed
ρ_{MT}	Shedding of virus into the bacteria concentration from malaria/typhoid	10	Assumed

The model is formulated under the following assumptions:

1. The human population is assumed to be homogeneous, such that individuals have an equal likelihood of interacting with one another.
2. Additional mortality due to the diseases is considered in all infected and infectious human compartments.
3. New individuals enter the human population through births and immigration.
4. Individuals who recover from either disease may lose their immunity and become susceptible to re-infection.

Using figure 1, the variables and parameters in table 1 and 2 respectively, yields the malaria fever and typhoid co-infection as stated below:

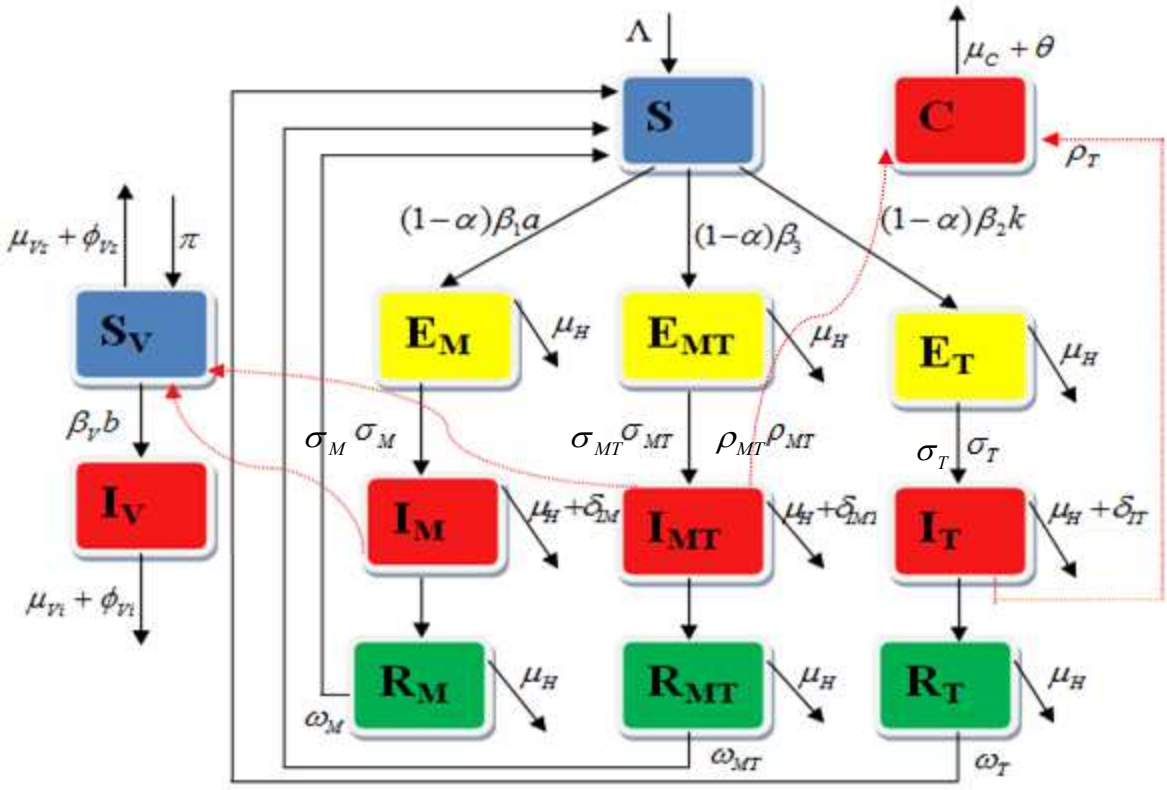


Figure 1: Malaria-Typhoid co-infection Flow Diagram

$$
\left.
\begin{aligned}
\frac{dS}{dt} &= \Lambda - (1-\alpha)\frac{(\beta_1 a I_V + \beta_2 k I_T + \beta_3 I_{MT})}{N_H} S - \mu_H S + \omega_M R_M + \omega_T R_T + \omega_{MT} R_{MT} \\
\frac{dE_M}{dt} &= (1-\alpha)\frac{(\beta_1 a I_V)}{N_H} S - (\sigma_M + \mu_H) E_M \\
\frac{dE_T}{dt} &= (1-\alpha)\frac{(\beta_2 k I_T)}{N_H} S - (\sigma_T + \mu_H) E_T \\
\frac{dE_{MT}}{dt} &= (1-\alpha)\frac{(\beta_3 I_{MT})}{N_H} S - (\sigma_{MT} + \mu_H) E_{MT} \\
\frac{dI_M}{dt} &= \sigma_M E_M - (\gamma_M + \mu_H + \delta_{IM}) I_M \\
\frac{dI_T}{dt} &= \sigma_T E_T - (\gamma_T + \mu_H + \delta_{IT}) I_T \\
\frac{dI_{MT}}{dt} &= \sigma_{MT} E_{MT} - (\gamma_{MT} + \mu_H + \delta_{IMT}) I_{MT} \\
\frac{dR_M}{dt} &= \gamma_M I_M - (\omega_M + \mu_H) R_M \\
\frac{dR_T}{dt} &= \gamma_T I_T - (\omega_T + \mu_H) R_T \\
\frac{dR_{MT}}{dt} &= \gamma_{MT} I_{MT} - (\omega_{MT} + \mu_H) R_{MT} \\
\frac{dS_V}{dt} &= \pi - \frac{\beta_V b I_M S_V}{N_V} - (\mu_{Vs} + \phi_{Vs}) S_V \\
\frac{dI_V}{dt} &= \frac{\beta_V b I_M S_V}{N_V} - (\mu_{Vi} + \phi_{Vi}) I_V \\
\frac{dC}{dt} &= \rho_T I_T + \rho_{MT} I_{MT} - (\mu_C + \theta) C
\end{aligned}
\right\} \qquad (4)
$$

For simplicity and better analysis, let

$$
K_1 = (\sigma_M + \mu_H), \quad K_2 = (\sigma_T + \mu_H), \quad K_3 = (\sigma_{MT} + \mu_H), \quad K_4 = (\gamma_M + \mu_H + \delta_{IM}),
$$

$$
K_5 = (\gamma_T + \mu_H + \delta_{IT}), \; K_6 = (\gamma_{MT} + \mu_H + \delta_{IMT}), \quad K_7 = (\omega_M + \mu_H), K_8 = (\omega_T + \mu_H),
$$

$$
K_9 = (\omega_{MT} + \mu_H), \quad K_{10} = (\mu_{Vs} + \phi_{Vs}), \quad K_{11} = (\mu_{Vi} + \phi_{Vi}), \quad K_{12} = (\mu_C + \theta)
$$

$$
\lambda_1 = \left(\lambda_2 + \lambda_3 + \lambda_4\right), \; \lambda_2 = \frac{(\beta_1 a I_V)}{N_H}, \; \lambda_3 = \frac{(\beta_2 k I_T)}{N_H}, \; \lambda_4 = \frac{(\beta_3 I_{MT})}{N_H}, \; \lambda_5 = \frac{\beta_V b I_M}{N_V}
$$

$$\left.\begin{aligned}
\frac{dS}{dt} &= \Lambda - (1-\alpha)\lambda_1 S - \mu_H S + \omega_M R_M + \omega_T R_T + \omega_{MT} R_{MT} \\
\frac{dE_M}{dt} &= (1-\alpha)\lambda_2 S - K_1 E_M \\
\frac{dE_T}{dt} &= (1-\alpha)\lambda_3 S - K_2 E_T \\
\frac{dE_{MT}}{dt} &= (1-\alpha)\lambda_4 S - K_3 E_{MT} \\
\frac{dI_M}{dt} &= \sigma_M E_M - K_4 I_M \\
\frac{dI_T}{dt} &= \sigma_T E_T - K_5 I_T \\
\frac{dI_{MT}}{dt} &= \sigma_{MT} E_{MT} - K_6 I_{MT} \\
\frac{dR_M}{dt} &= \gamma_M I_M - K_7 R_M \\
\frac{dR_T}{dt} &= \gamma_T I_T - K_8 R_T \\
\frac{dR_{MT}}{dt} &= \gamma_{MT} I_{MT} - K_9 R_{MT} \\
\frac{dS_V}{dt} &= \pi - \lambda_5 S_V - K_{10} S_V \\
\frac{dI_V}{dt} &= \lambda_5 S_V - K_{11} I_V \\
\frac{dC}{dt} &= \rho_T I_T - K_{12} C
\end{aligned}\right\} \qquad (5)$$

3.0. Basic properties of the model

3.0.1. Invariant region of the Malaria-Typhoid co-infection model

Theorem 3.0. Let the initial solution set $S(0), E_M(0), E_T(0), E_{MT}(0), I_M(0), I_T(0), I_{MT}(0), R_M(0), R_T(0), R_{MT}(0), S_V(0), I_V(0), C(0) > 0$ be non-negative initial conditions, then system (4) has a nonnegative solution $S(t), E_M(t), E_T(t), E_{MT}(t), I_M(t), I_T(t), I_{MT}(t), R_M(t), R_T(t), R_{MT}(t), S_V(t), I_V(t), C(t)$ for all $t > 0$. Moreover, $\underset{t\to\infty}{Lim\,Sup}\ N_H(t) \le \frac{\Lambda}{\mu_H}$, $\underset{t\to\infty}{Lim\,Sup}\ N_V(t) \le \frac{\pi}{\mu_{Vs} + \phi_{Vs}}$, $\underset{t\to\infty}{Lim\,Sup}\ N_C(t) \le \frac{\rho_T}{\mu_C + \theta}$. In

addition, if $N_H(0) \le \frac{\Lambda}{\mu_H}$,then $N_H(t) \le \frac{\Lambda}{\mu_H}$, $N_V(0) \le \frac{\pi}{\mu_{Vs} + \phi_{Vs}}$, then $N_V(t) \le \frac{\pi}{\mu_{Vs} + \phi_{Vs}}$ and $N_B(0) \le \frac{\rho_T}{\mu_C + \theta}$ then, $N_B(t) \le \frac{\rho_T}{\mu_C + \theta}$. Therefore, the feasible region of system (4) given as:

$$D_H \times D_V \times D_C \in \Re_+^{10} \times \Re_+^2 \times \Re_+ \tag{6}$$

Where;

$$D_H = \left\{ S, E_M, E_T, E_{MT}, I_M, I_T, I_{MT}, R_M, R_T, R_{MT} \in \Re_+^{10} : N_H \le \frac{\Lambda}{\mu_H} \right\} \tag{7}$$

$$D_V = \left\{ S_V, I_V \in \Re_+^2 : N_V \le \frac{\pi}{\mu_{VS} + \phi_{VS}} \right\} \tag{8}$$

$$D_C = \left\{ C \in \Re_+ : N_C \le \frac{\rho_T}{\mu_C + \theta} \right\} \tag{9}$$

is positively invariant and attracting.

Proof. Considering the first equation in system (4), we obtain the following:

$$\frac{dS}{dt} = (1-\alpha)\frac{(\beta_1 a I_V + \beta_2 k I_T + \beta_3 I_{MT})}{N_H} S + \mu_H S \ge 0 \tag{10}$$

From time $t = 0$ to $t = t$, we integrated (10) to get;

$$\frac{d}{dt}\left[S(t) \exp\left\{ \int_0^t (1-\alpha)\frac{(\beta_1 a I_V + \beta_2 k I_T + \beta_3 I_{MT})}{N_H} + \mu_H \right\} \right] \ge 0$$

This implies that;

$$S(t) \ge S(0) \exp\left\{ -\left(\int_0^t (1-\alpha)\frac{(\beta_1 a I_V + \beta_2 k I_T + \beta_3 I_{MT})}{N_H} + \mu_H \right) \right\} > 0, \forall t > 0.$$

A similar approach was employed to demonstrate that $E_M(t), E_T(t), E_{MT}(t), I_M(t), I_T(t), I_{MT}(t), R_M(t), R_T(t), R_{MT}(t), S_V(t), I_V(t), C(t) > 0$ remain positive for all $t > 0$. The second part of Theorem 1 is proven by summing the human and mosquito compartments of (4) separately with $\delta_{IM} = \delta_{IT} = \delta_{IMT} = 0$:

$$\frac{dN_H}{dt} = \Lambda - \mu_H N_H$$

This implies that $N_H(t) = N_H(0)\exp^{-\mu_H t} + \frac{\Lambda}{\mu_H}(1-\exp^{-\mu_H t})$. Thus, $\underset{t\to\infty}{Lim\,Sup}\ N_H(t) \le \frac{\Lambda}{\mu_H}$

Similarly, we establish the corresponding results for the vector and bacterial populations. If $N_V(t) = N_V(0)\exp^{-(\mu_{Vs}+\phi_{Vs})t} + \frac{\pi}{\mu_{Vs}+\phi_{Vs}}(1-\exp^{-(\mu_{Vs}+\phi_{Vs})t})$. Thus, $\underset{t\to\infty}{Lim\,Sup}\ N_V(t) \le \frac{\pi}{\mu_{Vs}+\phi_{Vs}}$, and $\underset{t\to\infty}{Lim\,Sup}\ N_C \le \frac{\rho_T + \rho_{MT}}{\mu_C + \theta}$. Thus, the boundedness of the solutions within D is proven, and the solutions to system (4) are positively invariant and attract in this region. Additionally, system (4) is both biologically valid and mathematically well-posed within D.

3.1. Analysis of Sub-Models

The model is first divided into separate malaria and typhoid sub-models to understand each disease's dynamics, and then combined to analyze their interaction in a co-infection framework.

3.1.1 Analysis of Malaria Model Only

To analyze malaria dynamics, the malaria and co-infection compartments are removed from system (4), resulting in a simplified malaria-only sub-model. Hence;

$$\left.\begin{aligned}
\frac{dS}{dt} &= \Lambda - (1-\alpha)\lambda_2 S - \mu_H S + \omega_M R_M \\
\frac{dE_M}{dt} &= (1-\alpha)\lambda_2 S - K_1 E_M \\
\frac{dI_M}{dt} &= \sigma_M E_M - K_4 I_M \\
\frac{dR_M}{dt} &= \gamma_M I_M - K_7 R_M \\
\frac{dS_V}{dt} &= \pi - \lambda_5 S_V - K_{10} S_V \\
\frac{dI_V}{dt} &= \lambda_5 S_V - K_{11} I_V
\end{aligned}\right\} \qquad (11)$$

3.1.2. *Stability analysis of malaria disease-free equilibrium (DFE), endemic equilibrium and basic reproduction number (R_0^M)*

By setting the derivatives in equation (11) to zero, the disease-free equilibrium for malaria model only is obtained as follows:

$$E_{0M} = (S_0, E_{M0}, I_{M0}, R_{M0}, S_{V0}, I_{V0}) = \left(\frac{\Lambda}{\mu_H}, 0, 0, 0, \frac{\pi}{K_{10}}, 0\right) \qquad (12)$$

To establish the existence of an endemic equilibrium for the malaria-only sub-model (11), let

$\varepsilon_M^* = \left(S^*, E_M^*, I_M^*, R_M^*, S_V^*, I_V^*\right)$ denote the endemic equilibrium, where all state variables are positive. Setting the right-hand sides of system (11) to zero gives the equilibrium conditions as obtained below;

At equilibrium:

$$E_M^* = \frac{K_4}{\sigma_M} I_M^*,\ R_M^* = \frac{\gamma_M}{K_7} I_M^*,\ S_V^* = \frac{\pi N_V}{\beta_V b I_M^* + K_{10} N_V},\ I_V^* = \frac{\beta_V b \pi I_M^*}{K_{11}(\beta_V b I_M^* + K_{10} N_V)} \quad (13)$$

the equilibrium condition can be reduced to an equation involving only I_M^*

$$H = \frac{K_4}{\sigma_M} + 1 + \frac{\gamma_M}{K_7} \text{ and } F = \frac{K_1 K_4}{\sigma_M} - \frac{\omega_M \gamma_M}{K_7}$$

Since $N_H^* = S^* + H I_M^*$

Therefore; $S^* = \frac{\Lambda - F I_M^*}{\mu_H}$

On substituting S^* into the remaining equilibrium relation and simplifying, we obtain the following quadratic equation in I_M^* ;

$$A(I_M^*)^2 + B I_M^* + C = 0$$

$$A = \frac{\beta_V b \delta_M}{\pi}, B = \delta_M - \frac{\beta_V b \Lambda}{\pi} - \left(R_0^M\right)^2 \left(\frac{K_1 K_4}{\sigma_M} - \frac{\omega_M \gamma_M}{K_7}\right), C = \Lambda\left(\left(R_0^M\right)^2 - 1\right)$$

Therefore, the endemic infected population is

$$I_M^* = \frac{-B + \sqrt{B^2 - 4AC}}{2A}$$

subject to $I_M^* < \frac{\Lambda}{F}$, which ensures $S^* > 0$.

Since $\Lambda > 0$, therefore $C > 0$ and this implies $\left(R_0^M\right)^2 > 1$

Consequently, $R_0^M > 1$ is the threshold condition for the existence of a positive endemic equilibrium.

Therefore, the malaria-only model admits a biologically feasible endemic equilibrium $\varepsilon_M^* = \left(S^*, E_M^*, I_M^*, R_M^*, S_V^*, I_V^*\right)$ whenever $R_0^M > 1$.

To compute the basic reproduction number (R_0^M) for the system (11), the next-generation matrix method is employed. This approach involves constructing two matrices F , which represents the rate of new infections, and V , which accounts for all other transition terms [16, 17]. The effective reproduction number is then defined as $R_0^M = \rho(FV^{-1})$.

Where ρ denotes the spectral radius of the matrix. Thus at disease free, from equation (11), we derived

$$F = \begin{pmatrix} (1-\alpha)\beta_1 a \dfrac{I_V}{N_H} S \\ 0 \\ \beta_V b \dfrac{I_M}{N_V} S_V \end{pmatrix}, V = \begin{pmatrix} K_1 E_M \\ -\sigma_M E_M + K_4 I_M \\ K_{11} I_V \end{pmatrix} \tag{14}$$

Differentiating (14) with respect to E_M, I_M, I_V respectively at the disease free equilibrium and

The matrices V^{-1} and (FV^{-1}) are obtained. Hence

$$R_0^M = \rho(FV^{-1}) = \sqrt{\frac{\beta_1 a \beta_V b \sigma_M (1-\alpha)}{K_1 K_4 K_{11}}} \tag{15}$$

3.1.3. *Global Stability of Disease-Free Equilibrium of the malaria model (GSDFE)*

Theorem 3.2. The disease-free equilibrium (DFE) is globally asymptotically stable if all trajectories of the system converge to the (DFE) as time approaches infinity, provided the basic reproduction number R_0^M is less than one, i.e. $R_0^M < 1$ and when R_0^M is greater than one, i.e. $R_0^M > 1$, it is globally asymptotically unstable.

Proof 3.2. Using infected compartment of (11), for DFE as adopted in [17]

Let L denote the Lyapunov function which is given by;

$\dot{L} = A\dot{E}_M + B\dot{I}_M + C\dot{I}_V$

$$\dot{L} = K_{11}\left((1-\alpha)\lambda_2 S - K_1 E_M\right) + \frac{K_1 K_{11}}{\sigma_M}\left(\sigma_M E_M - K_4 I_M\right) + (1-\alpha)\lambda_2 S\left(\lambda_5 S_V - K_{11} I_V\right)$$

$$\dot{L} = \left((1-\alpha)\lambda_2\lambda_5 - \frac{K_1 K_4 K_{11}}{\sigma_M}\right) I_M \quad (16)$$

Substitute $\lambda_2\lambda_5$ into equation (16) and rewrite it in term of R_0^M obtained in equation (15)

$$\dot{L} = \left(\frac{\sqrt{R_0^M}\, K_1 K_4 K_{11}}{\sigma_M} - \frac{K_1 K_4 K_{11}}{\sigma_M}\right) I_M$$

$$\dot{L} = \left(\left(R_0^M - 1\right)\sqrt{\frac{K_1 K_4 K_{11}}{\sigma_M}}\right) I_M$$

Hence, $\dot{L} < 0$ whenever $R_0^M < 1$, and $\dot{L} = 0$ if and only if $E_M = I_M = I_V = 0$

Moreover, the largest invariant set contained in $\left\{\left(S, E_M, I_M, R_M, S_V, I_V\right) \in D : \dot{L} = 0\right\}$ is the singleton $\left\{E_M^0\right\}$. By LaSalle's Invariance Principle [23], every solution of the model with initial conditions in D converges to E_M^0 as $t \to \infty$. Consequently, the disease-free equilibrium is globally asymptotically stable whenever $R_0^M < 1$

The epidemiological implication of Theorem 3.2. is that malaria can be completely eradicated from the community, irrespective of the initial sizes of the model subpopulations, provided that the basic reproduction number remains below unity.

3.1.4. *Global stability analysis of endemic equilibrium of the malaria model (GSEE)*

The global stability of the endemic equilibrium of the malaria model is considered here, and for the malaria model only admits a biologically feasible endemic equilibrium E_M^* with all components strictly positive (requires $R_0^M > 1$)

Theorem 3.3: Suppose $R_0^M > 1$, the unique endemic equilibrium E_M^* of the co-infection model exists, then E_M^* is globally asymptotically stable in the interior of D.

Proof

The Volterra type of Lyapunov function is used to prove the global stability of the endemic equilibrium, for the case $\omega_M = 0$.

$$L = \left(S - S^* - S^* \ln \frac{S}{S^*} \right) + \left(E_M - {E_M}^* - {E_M}^* \ln \frac{E_M}{{E_M}^*} \right) + \frac{\sigma_M}{K_4} \left(I_M - {I_M}^* - {I_M}^* \ln \frac{I_M}{{I_M}^*} \right)$$
$$+ \left(S_V - {S_V}^* - {S_V}^* \ln \frac{S_V}{{S_V}^*} \right) + \left(I_V - {I_V}^* - {I_V}^* \ln \frac{I_V}{{I_V}^*} \right) \tag{17}$$

Taking the derivative of (17), we have

$$\dot{L} = \left(1 - \frac{S^*}{S} \right) \dot{S} + \left(1 - \frac{{E_M}^*}{E_M} \right) \dot{E_M} + \frac{\sigma_M}{K_4} \left(1 - \frac{{I_M}^*}{I_M} \right) \dot{I_M} + \left(1 - \frac{{S_V}^*}{S_V} \right) \dot{S_V} + \left(1 - \frac{{I_V}^*}{I_V} \right) \dot{I_V} \tag{18}$$

Substitute equation 11 into (18), gives;

$$\dot{L} = \left(1 - \frac{S^*}{S} \right) \left(\Lambda - (1-\alpha)\lambda_2 S - \mu_H S \right) + \left(1 - \frac{{E_M}^*}{E_M} \right) \left((1-\alpha)\lambda_2 S - K_1 E \right) +$$
$$\frac{\sigma_M}{K_4} \left(1 - \frac{{I_M}^*}{I_M} \right) \left(\sigma_M E_M - K_4 I \right) + \left(1 - \frac{{S_V}^*}{S_V} \right) \left(\pi - \lambda_5 S_V - K_{10} S_V \right) + \left(1 - \frac{{I_V}^*}{I_V} \right) \left(\lambda_5 S_V - K_{11} I_V \right) \tag{19}$$

Expand (19), gives;

$$\dot{L} = \left(\Lambda - (1-\alpha)\lambda_2 S - \mu_H S - \frac{S^*}{S}\Lambda + (1-\alpha)\lambda_2 S^* + \mu_H S^* \right) +$$
$$\left((1-\alpha)\lambda_2 S - K_1 E_M - (1-\alpha)\lambda_2 \frac{{E_M}^*}{E_M} S - K_1 {E_M}^* \right) +$$
$$\left(\frac{{\sigma_M}^2}{K_4} E_M - \sigma_M + \frac{{\sigma_M}^2}{K_4} \frac{{I_M}^*}{I_M} E_M + \sigma_M \frac{{I_M}^*}{I_M} I \right) +$$
$$\left(\pi - \lambda_5 S_V - K_{10} - \pi \frac{{S_V}^*}{S_V} + \lambda_5 {S_V}^* + K_{10} \frac{{S_V}^*}{S_V} \right) + \left(\lambda_5 S_V - K_{11} - \lambda_5 S_V \frac{{I_V}^*}{I_V} + K_{11} {I_V}^* \right) \tag{20}$$

Simplifying and factorizing Equation (20), gives;

$$\dot{L} = \mu_H S^* \left(2 - \frac{S^*}{S} - \frac{S}{S^*} \right) - K_1 {E_M}^* \left(4 - \frac{E_M}{{E_M}^*} - \frac{{E_M}^*}{E_M} \right) - \sigma_M {I_M}^* \left(4 - \frac{I_M}{{I_M}^*} - \frac{{I_M}^*}{I_M} \right) -$$
$$\mu_V {S_V}^* \left(2 - \frac{S_V}{{S_V}^*} - \frac{{S_V}^*}{S_V} \right) - \mu_V {I_V}^* \left(2 - \frac{I_V}{{I_V}^*} - \frac{{I_V}^*}{I_V} \right) \tag{21}$$

Since all model parameters are positive, it follows that $L < 0$. Hence, by the LaSalle Invariance Principle [17], every solution of the model converges to the endemic equilibrium E_M^* as $t \to \infty$ whenever $R_0^M > 1$.

Theorem 3.3 implies that malaria/typhoid co-infection remains endemic in the community, independent of the initial population sizes, whenever $R_0^M > 1$.

3.1.5. *Sensitivity analysis of malaria fever model*

In this section, sensitivity analysis is carried out to study the effect of parameter variations on model outcomes, highlighting the most influential parameters and confirming the stability of the model results under uncertainty.

The normalized forward sensitivity index of R_0^M with respect to a parameter w is defined as:

$$X_w^{R_0^M} = \frac{\partial R_0^M}{\partial w}\frac{w}{R_0^M} \qquad (22)$$

The results obtained are presented in table 4 showing the indices of all parameters in R_0^M

Table 3. Sensitivity index of R_0^M

Parameters	Sensitivity Expression	Value	Index
α	$-\frac{1}{2}\left(\frac{\alpha}{1-\alpha}\right)$	-0.5	-
β_1	$\frac{1}{2}$	0.5	+
β_V	$\frac{1}{2}$	0.5	+
a	$\frac{1}{2}$	0.5	+
b	$\frac{1}{2}$	0.5	+
σ_M	$\frac{1}{2}\left(\frac{\mu_H}{K_1}\right)$	0.0432	+
γ_M	$-\frac{1}{2}\frac{\gamma_M}{K_4}$	-0.46095	-
μ_H	$-\frac{1}{2}\frac{(K_4)\mu_H + \mu_H}{K_1 K_4}$	-0.07802	-
μ_{VI}	$-\frac{1}{2}\frac{\mu_{VI}}{K_{11}}$	-0.1613	-
δ_{IM}	$-\frac{1}{2}\frac{\delta_{IM}}{K_4}$	-0.00420	-
ϕ_{VI}	$-\frac{1}{2}\frac{\phi_{VI}}{K_{11}}$	-0.3387	-

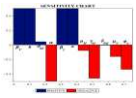


Figure 2: Bar chart showing the sensitivity indices of the effective reproduction number (R_0^M), indicating the relative influence of model parameters on malaria transmission.

A sensitivity analysis was conducted to determine how changes in model parameters affect the effective reproduction number, R_0^M , which measures the potential spread of malaria in the population. The results indicate that some parameters have a **positive influence** on R_0^M , meaning that an increase in their values leads to a higher potential for disease transmission. These parameters include the transmission probability from humans to mosquitoes (β_V), the transmission probability from mosquitoes to humans (β_1), the mosquito biting rate (a), the number of humans bitten per mosquito per unit time (b), and the progression rate from exposed to infectious humans (σ_M). An increase in any of these parameters enhances the contact or transmission efficiency between humans and mosquitoes, thereby raising R_0^M .

Conversely, other parameters exhibit a **negative influence** on R_M^0 , meaning that increasing their values reduces the spread of malaria. These include the environmental sanitation factor (α), which reduces transmission through improved hygiene and sanitation; the natural death rate of humans (μ_H) and mosquitoes (μ_V); the recovery rate of infected humans (γ_M); the malaria-induced death rate of humans (δ_{IM}); and mosquito mortality due to insecticide spraying (ϕ_V). Higher values of these parameters either reduce the number of susceptible or infectious individuals in the population or limit the survival of the vector, thereby decreasing R_{0M} .

Overall, the sensitivity analysis highlights that interventions targeting vector control (such as increasing ϕ_V and μ_V) and improving human recovery and environmental sanitation (through

γ_M and α) are crucial in reducing malaria transmission. Meanwhile, factors that enhance transmission efficiency, such as mosquito biting rates or transmission probabilities (a, b, β_1, β_V), should be carefully monitored, as increases in these parameters can significantly raise R_{0M}.

3.2.1. *Analysis of Typhoid Model Only*

To focus on the typhoid dynamics, the malaria and co-infection compartments are removed from system (4), yielding a simplified model specific to typhoid model only.

$$\left.\begin{aligned}
\frac{dS}{dt} &= \Lambda - (1-\alpha)\lambda_3 S - \mu_H S + \omega_T R_T \\
\frac{dE_T}{dt} &= (1-\alpha)\lambda_3 S - K_2 E_T \\
\frac{dI_T}{dt} &= \sigma_T E_T - K_5 I_T \\
\frac{dR_T}{dt} &= \gamma_T I_T - K_8 R_T \\
\frac{dC}{dt} &= \rho_T I_T - K_{12} C
\end{aligned}\right\} \quad (23)$$

3.2.2.*Stability analysis of typhoid disease-free equilibrium (DFE), endemic equilibrium (EE), and basic reproduction number (R_0^T)*

By setting the derivatives in equation (23) to zero, the disease-free equilibrium is obtained as follows:

$$E_{0T} = \left(S_0, E_{T0}, I_{T0}, R_{T0}, C_0\right) = \left(\frac{\Lambda}{\mu}, 0, 0, 0, 0\right) \quad (24)$$

The endemic equilibrium point of (23) is given by:

$$E_T^* = \left(\begin{aligned}
&\frac{\Lambda + \omega_T R_T^*}{(1-\alpha)\lambda_3 + \mu}, \frac{(1-\alpha)\lambda_3 S^*}{K_2}, \\
&\frac{\sigma_T E_T^*}{K_5}, \frac{\gamma_T I_T^*}{K_8}, \frac{\rho_T I_T^*}{K_{12}}
\end{aligned}\right) \quad (25)$$

To compute the basic reproduction number (R_0^T) for the system (23), the next-generation matrix method is employed. This approach involves constructing two matrices: F, which represents the rate of new infections, and V, which accounts for all other transition terms. The basic reproduction number is then defined as

$$F = \begin{pmatrix} (1-\alpha)\beta_2 k \dfrac{I_T}{N_H} S \\ 0 \\ 0 \end{pmatrix}, V = \begin{pmatrix} K_2 E_T \\ -\sigma_T E_T + K_5 I_T \\ -\rho_T I_T + K_{12} C \end{pmatrix} \quad (26)$$

Differentiating (16) with respect to E_T, I_T, C respectively at the disease free equilibrium, and the matrices V^{-1} and (FV^{-1}) are obtained. Hence;

$$R_0^T = \rho(FV^{-1}) = \frac{\beta_2 k \sigma_T (1-\alpha)}{K_2 K_5} \quad (27)$$

3.2.3. *Global Stability of Disease-Free Equilibrium of the typhoid model (GSDFE)*

Theorem 3.4 The disease-free equilibrium (DFE) is globally asymptotically stable if all trajectories of the system converge to the (DFE) as time approaches infinity, provided the basic reproduction number R_{0T} is less than one $\left(R_0^T < 1\right)$ and when R_0^T is greater than one $\left(R_0^T > 1\right)$it is Globally asymptotically unstable.

Proof: Let $L = AE_T + BI_T$

Differentiating, we have:

$L^I = AE_T^I + BI_T^I$

$L^I = A\left((1-\alpha)\lambda_3 S - K_2 E_T\right) + B\left(\sigma_T E_T - K_5 I_T\right)$

Solving, we have:

$A = K_5, B = (1-\alpha)\lambda_3$

Therefore:

$L^I = K_5\left((1-\alpha)\lambda_3 S - K_2 E_T\right) + (1-\alpha)\lambda_3\left(\sigma_T E_T - K_5 I_T\right)$

$L^I = \left(-K_2 K_5 + (1-\alpha)\lambda_3 \sigma_T\right)E_T \quad (28)$

Rewrite equation (28) it in term of R_0^T to obtain equation (29)

$L^I = \left(R_0^T K_2 K_5 - K_2 K_5\right)E_T \quad (29)$

Therefore:

$L^I = \left(R_0^T - 1\right)K_2 K_5 E_T$

Hence; $L^I \le 0$

In particular, $L^I < 0$, if $R_0^T < 1$, and $L^I = 0$, if $E_T = 0$

3.2.4. *Global stability analysis of endemic equilibrium of the typhoid model*

The global stability of the endemic equilibrium of the typhoid model is considered here, and for the typhoid model only admits a biologically feasible endemic equilibrium E_T^* with all components strictly positive (requires $R_0^T > 1$)

Theorem 3.5: Suppose $R_0^T > 1$, the unique endemic equilibrium E_T^* of the co-infection model exists. Then E_T^* is globally asymptotically stable in the interior of D.

Proof

The Volterra type of Lyapunov function is used to prove the global stability of the endemic equilibrium for the case $\omega_T = 0$. From (23)

$$L = \left(S - S^* - S^* \ln\frac{S}{S^*}\right) + \left(E_T - E_T^* - E_T^* \ln\frac{E_T}{E_T^*}\right) + \left(I_T - I_T^* - I_T^* \ln\frac{I_T}{I_T^*}\right) + \left(C - C^* - C^* \ln\frac{C}{C^*}\right) \quad (30)$$

Taking the derivative of (30), we have

$$\dot{L} = \left(1 - \frac{S^*}{S}\right)\dot{S} + \left(1 - \frac{E_T^*}{E_T}\right)\dot{E}_T + \left(1 - \frac{I_T^*}{I_T}\right)\dot{I}_T + \left(1 - \frac{C^*}{C}\right)\dot{C} \quad (31)$$

Substitute equation 23 into (31), gives;

$$\dot{L} = \left(1 - \frac{S^*}{S}\right)\left(\Lambda - (1-\alpha)\lambda_3 S - \mu_H S\right) + \left(1 - \frac{E_T^*}{E_T}\right)\left((1-\alpha)\lambda_3 S - K_2 E_T\right) + \left(1 - \frac{I_T^*}{I_T}\right)\left(\sigma_T E_T - K_5 I_T\right) + \left(1 - \frac{C^*}{C}\right)\left(\rho_T I_T - K_{12} C\right) \quad (32)$$

Expand (32), gives;

$$\dot{L} = \left(\Lambda - (1-\alpha)\lambda_3 S - \mu_H S - \Lambda\frac{S^*}{S} + (1-\alpha)\lambda_3 S^* + \mu_H S^*\right) + \left((1-\alpha)\lambda_3 S - K_2 E_T - (1-\alpha)\lambda_3 S\frac{E_T^*}{E_T} + K_2 E_T^*\right) + \left(\sigma_T E_T - K_5 I_T - \sigma_T E_T\frac{I_T^*}{I_T} + K_5 I_T^*\right) + \left(\rho_T I_T - K_{12} C - \rho_T I_T\frac{C^*}{C} + K_{12} C^*\right) \quad (33)$$

Simplifying and factorizing Equation (33), gives;

$$\dot{L} = -\mu_H S^*\left(\frac{S}{S^*} + \frac{S^*}{S} - 2\right) - K_2 E_T^*\left(\frac{E_T}{E_T^*} + \frac{E_T^*}{E_M} - 2\right) - K_5 I_T^*\left(\frac{I_T}{I_T^*} + \frac{I_T^*}{I_T} - 2\right) - K_{12} C^*\left(\frac{C}{C^*} + \frac{C^*}{C} - 2\right) \quad (34)$$

Since all model parameters are positive, it follows that $L < 0$. Hence, by the LaSalle Invariance Principle [17], every solution of the model converges to the endemic equilibrium E_T^* as $t \to \infty$ whenever $R_0^T > 1$.

Theorem 5 implies that typhoidinfection remains endemic in the community, independent of the initial population sizes, whenever $R_0^T > 1$.

3.2.5. *Sensitivity analysis of typhoid fever model*

The normalized forward sensitivity index of R_{0T} with respect to a parameter $x \in R_{0T}$ is defined as:

$$\frac{\partial R_0^T}{\partial x} \times \frac{x}{R_0^T} \qquad (35)$$

Table 4: Sensitivity indices quantifying the influence of model parameters on R_T^0.

Parameter	Sensitivity Expression	Value	Index
β_2	1	1	+
k	1	1	+
σ_T	$\frac{\mu_H}{K_2}$	0.0950	+
α	$-\left(\frac{\alpha}{1-\alpha}\right)$	-1	-
μ_H	$-\frac{(K_5)\mu_H + \mu_H}{K_2 K_5}$	0.0969	+
γ_T	$-\frac{\gamma_T}{K_5}$	-0.0196	-
δ_{IT}	$-\frac{\delta_{IT}}{K_5}$	-0.00023	-
ρ_T	$-\frac{\rho_T}{K_5}$	-0.9783	-

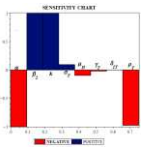


Figure 3: Bar chart showing the sensitivity indices of the effective reproduction number (R_{0T}), indicating the relative influence of model parameters on typhoid transmission.

3.3.0 *Analysis of the co-infection model*

3.3.1.*Stability analysis of malaria-typhoid co-infection disease-free equilibrium (DFE) and basic reproduction number (R_0^{MT})*

The disease free equilibrium points represent the steady state solutions where the malaria/typhoid disease is absent from the system (5), i.e., when $E_M = E_T = E_{MT} = I_M = I_T = I_{MT} = R_M = R_T = R_{MT} = I_V = C = 0$. The disease free equilibrium is obtained by setting the left hand side of the equations (5) to 0. Let E^0 denote the disease free equilibrium point, then at disease free:

$$E_F{}^0 = \left(\frac{\Lambda}{\mu_H}, 0,0,0,0,0,0,0,0,0, \frac{\pi}{K_{10}}, 0,0 \right) \qquad (36)$$

The effective reproduction number is defined as the average number of secondary infections produced by a malaria–typhoid infectious individual in a population where a proportion of

individuals may already be immune or protected through vaccination and other intervention strategies [16, 17]. Mathematically, it is given by;

$$R_0^{MT} = \rho\left(FV^{-1}\right) \tag{37}$$

Where F denotes the matrix of new infection terms V represents the matrix of all other transition terms in the system. Hence, we have;

$$F = \begin{pmatrix} (1-\alpha)\beta_1 a \dfrac{I_V}{N_H} S \\ (1-\alpha)\beta_2 k \dfrac{I_T}{N_H} S \\ (1-\alpha)\beta_3 \dfrac{I_{MT}}{N_H} S \\ 0 \\ 0 \\ 0 \\ \beta_V b \dfrac{I_M}{N_V} S_V \\ 0 \end{pmatrix} \tag{38}$$

$$V = \begin{pmatrix} K_1 E_M \\ K_2 E_T \\ K_3 E_{MT} \\ -\sigma_M E_M + K_4 I_M \\ -\sigma_T E_T + K_5 I_T \\ -\sigma_{MT} E_{MT} + K_6 I_{MT} \\ K_{11} I_V \\ -\rho_T I_T - \rho_{MT} I_{MT} + K_{12} C \end{pmatrix} \tag{39}$$

$$V^{-1}=\begin{pmatrix} \frac{1}{K_1} & 0 & 0 & 0 & 0 & 0 & 0 & 0 \\ 0 & \frac{1}{K_2} & 0 & 0 & 0 & 0 & 0 & 0 \\ 0 & 0 & \frac{1}{K_3} & 0 & 0 & 0 & 0 & 0 \\ \frac{\sigma_M}{K_1K_4} & 0 & 0 & \frac{1}{K_4} & 0 & 0 & 0 & 0 \\ 0 & \frac{\sigma_T}{K_2K_5} & 0 & 0 & \frac{1}{K_5} & 0 & 0 & 0 \\ 0 & 0 & \frac{\sigma_{MT}}{K_3K_6} & 0 & 0 & \frac{1}{K_6} & 0 & 0 \\ 0 & 0 & 0 & 0 & 0 & 0 & \frac{1}{K_{11}} & 0 \\ 0 & \frac{\rho_T\sigma_T}{K_1K_{12}} & \frac{\rho_{MT}\sigma_{MT}}{K_3K_6K_{12}} & 0 & \frac{\rho_T}{K_5K_{12}} & \frac{\rho_{MT}}{K_6K_{12}} & 0 & \frac{1}{K_{12}} \end{pmatrix} \tag{40}$$

$$R_0^{MT}=\rho\left(FV^{-1}\right)=\max\left(\frac{(1-\alpha)\beta_3\sigma_{MT}}{K_3K_6},\frac{(1-\alpha)\beta_2k\sigma_T}{K_2K_5},\sqrt{\frac{(1-\alpha)\beta_1a\beta_Vb\sigma_M}{K_1K_4K_{11}}}\right) \tag{41}$$

3.3.2.*Global stability of disease free equilibrium of the co-infection model*

Theorem 3.6: The disease-free equilibrium given by (5) is globally asymptotically stable whenever $R_0^{MT}<1$.

*Proof***:** To establish the global asymptotic stability of the disease-free equilibrium of the co-infection model, we construct an appropriate Lyapunov function as follows:

$$L=E_M+E_T+E_{MT}+\frac{K_1}{\sigma_M}I_M+\frac{K_2}{\sigma_T}I_T+\frac{K_3}{\sigma_{MT}}I_{MT}+\frac{K_1K_4}{\sigma_M\lambda_5^{\,0}}I_V+\frac{K_5K_2}{\rho_T\sigma_T}C \tag{42}$$

Differentiate equation (42), gives;

$$\dot{L}=\dot{E_M}+\dot{E_T}+\dot{E_{MT}}+\frac{K_1}{\sigma_M}\dot{I_M}+\frac{K_2}{\sigma_T}\dot{I_T}+\frac{K_3}{\sigma_{MT}}\dot{I_{MT}}+\frac{K_1K_4}{\sigma_M\lambda_5^{\,0}}\dot{I_V}+\frac{K_5K_2}{\rho_T\sigma_T}\dot{C}$$

$$\begin{aligned}\dot{L}=&\left[(1-\alpha)\lambda_2S-K_1E_M\right]+\left[(1-\alpha)\lambda_3S-K_2E_T\right]+\left[(1-\alpha)\lambda_4S-K_3E_{MT}\right]+\\&\frac{K_1}{\sigma_M}\left[\sigma_ME_M-K_4I_M\right]+\frac{K_2}{\sigma_T}\left[\sigma_TE_T-K_5I_T\right]+\frac{K_3}{\sigma_{MT}}\left[\sigma_{MT}E_{MT}-K_6I_{MT}\right]+\\&\frac{K_1K_4}{\sigma_M\beta_VS_V}\left[\lambda_5S_V-K_{11}I_V\right]+\frac{K_5K_2}{\rho_T\sigma_T}\left[\rho_TI_T-K_{12}C\right]\end{aligned} \tag{43}$$

$$\dot{L} = [(1-\alpha)\lambda_2 - K_1 E_M] + [(1-\alpha)\lambda_3 - K_2 E_T] + [(1-\alpha)\lambda_4 - K_3 E_{MT}] +$$
$$\frac{K_1}{\sigma_M}[\sigma_M E_M - K_4 I_M] + \frac{K_2}{\sigma_T}[\sigma_T E_T - K_5 I_T] + \frac{K_3}{\sigma_{MT}}[\sigma_{MT} E_{MT} - K_6 I_{MT}] + \quad (44)$$
$$\frac{K_1 K_4 K_{10}}{\sigma_M \lambda_5 \pi}[\lambda_5 - K_{11} I_V] + \frac{K_5 K_2}{\rho_T \sigma_T}[\rho_T I_T - K_{12} C]$$

$$\dot{L} = (1-\alpha)\lambda_2 + (1-\alpha)\lambda_3 + (1-\alpha)\lambda_4 + \frac{K_1 K_4}{\sigma_M}\left[\frac{K_{10}}{\pi} - 1\right] I_M - \frac{K_3 K_6}{\sigma_{MT}} I_{MT} - \frac{K_1 K_4 K_{10} K_{11}}{\sigma_M \lambda_5 \pi} I_V - \frac{K_2 K_5 K_{12}}{\rho_T \sigma_T} C$$

Since

$$R_{0F} = \rho\left(FV^{-1}\right) = \max\left(\frac{\lambda_4 \sigma_{MT}}{K_3 K_6}, \frac{\lambda_3 \sigma_T}{K_2 K_5}, \pm\frac{\sqrt{K_1 K_4 K_{11} \sigma_M \lambda_2 \lambda_5}}{K_1 K_4 K_{11}}\right)$$

Hence

$$\dot{L} \le \left(R_0^{MT} - 1\right)\left[\begin{array}{l}\left((1-\alpha)\lambda_2 - \frac{K_1 K_4 K_{10} K_{11}}{\sigma_M \lambda_5 \pi}\right) I_V + (1-\alpha)\lambda_3 + \left((1-\alpha)\beta_3 - \frac{K_3 K_6}{\sigma_{MT}}\right) I_{MT} + \\ \frac{K_1 K_4}{\sigma_M}\left[\frac{K_{10}}{\pi} - 1\right] I_M - - \frac{K_2 K_5 K_{12}}{\rho_T \sigma_T} C\end{array}\right] \quad (45)$$

Hence, $\dot{L} < 0$ whenever $R_{0F} < 1$, and $\dot{L} = 0$ if and only if $E_M = E_T = E_{MT} = I_M = I_T = I_{MT} = R_M = R_T = R_{MT} = I_V = C = 0$

Moreover, the largest invariant set contained in $\left\{(S, E_M, E_T, E_{MT}, I_M, I_T, I_{MT}, R_M, R_T, R_{MT}, S_V, I_V, C) \in D : \dot{L} = 0\right\}$ is the singleton $\left\{E_F{}^0\right\}$. By LaSalle's Invariance Principle [17], every solution of the model with initial conditions in D converges to $E_F{}^0$ as $t \to \infty$. Consequently, the disease-free equilibrium is globally asymptotically stable whenever $R_0^{MT} < 1$

The epidemiological implication of theorem 3.6 is that malaria-typhoid co-infection can be completely eradicated from the community, irrespective of the initial sizes of the model subpopulations, provided that the basic reproduction number remains below unity.

3.3.3. *Global stability of endemic equilibrium of the co-infection model*

The global stability of the endemic equilibrium of the model is considered here, and for the co-infection model admits a biologically feasible endemic equilibrium ε^* with all components strictly positive (requires $R_0^{MT} > 1$)

Theorem 3.7: Suppose $R_0^{MT} > 1$, the unique endemic equilibrium ε^* of the co-infection model exists. Then ε^* is globally asymptotically stable in the interior of D.

Proof

The Volterra type of Lyapunov function as adopted by [17] is used to prove the global stability of the endemic equilibrium, for the case $\omega_M, \omega_T, \omega_{MT} = 0$.

$$
\begin{aligned}
L &= \mu_H S^*\left(S - S^* - S^* \ln\frac{S}{S^*}\right) + \mu_{Vi} S_V{}^*\left(S_V - S_V{}^* - S_V{}^* \ln\frac{S_V}{S_V{}^*}\right) + \left(E_M - E_M{}^* - E_M{}^* \ln\frac{E_M}{E_M{}^*}\right) \\
&+ \frac{K_1}{\sigma_M}\left(I_M - I_M{}^* - I_M{}^* \ln\frac{I_M}{I_M{}^*}\right) + \left(E_T - E_T{}^* - E_T{}^* \ln\frac{E_T}{E_T{}^*}\right) + \frac{K_2}{\sigma_T}\left(I_T - I_T{}^* - I_T{}^* \ln\frac{I_T}{I_T{}^*}\right) \\
&+ \left(E_{MT} - E_{MT}{}^* - E_{MT}{}^* \ln\frac{E_{MT}}{E_{MT}{}^*}\right) + \frac{K_3}{\sigma_{MT}}\left(I_{MT} - I_{MT}{}^* - I_{MT}{}^* \ln\frac{I_{MT}}{I_{MT}{}^*}\right) \\
&+ K_{11}\left(I_V - I_V{}^* - I_V{}^* \ln\frac{I_V}{I_V{}^*}\right) + \left(C - C^* - C^* \ln\frac{C}{C^*}\right)
\end{aligned}
\tag{46}
$$

Taking the derivative of (46), we have

$$
\begin{aligned}
\dot{L} &= \mu_H S^*\left(1 - \frac{S^*}{S}\right)\dot{S} + \mu_{Vi} S_V{}^*\left(1 - \frac{S_V{}^*}{S_V}\right)\dot{S}_V + K_1 K_4\left(1 - \frac{E_M{}^*}{E_M}\right)\dot{E}_M + K_1\sigma_M\left(1 - \frac{I_M{}^*}{I_M}\right)\dot{I}_M \\
&+ K_2 K_5\left(1 - \frac{E_T{}^*}{E_T}\right)\dot{E}_T + K_2\sigma_T\left(1 - \frac{I_T{}^*}{I_T}\right)\dot{I}_T + K_3 K_6\left(1 - \frac{E_{MT}{}^*}{E_{MT}}\right)\dot{E}_{MT} + K_3\sigma_{MT}\left(1 - \frac{I_{MT}{}^*}{I_{MT}}\right)\dot{I}_{MT} \\
&+ K_{11}\left(1 - \frac{I_V{}^*}{I_V}\right)\dot{I}_V + K_{12}\left(1 - \frac{C^*}{C}\right)\dot{C}
\end{aligned}
\tag{47}
$$

$$
\begin{aligned}
\dot{L} &= \mu_H S^*\left(\dot{S} - \frac{S^*}{S}\dot{S}\right) + \mu_{Vi} S_V{}^*\left(\dot{S}_V - \frac{S_V{}^*}{S_V}\dot{S}_V\right) + K_1 K_4\left(\dot{E}_M - \frac{E_M{}^*}{E_M}\dot{E}_M\right) + K_1\sigma_M\left(\dot{I}_M - \frac{I_M{}^*}{I_M}\dot{I}_M\right) \\
&+ K_2 K_5\left(\dot{E}_T - \frac{E_T{}^*}{E_T}\dot{E}_T\right) + K_2\sigma_T\left(\dot{I}_T - \frac{I_T{}^*}{I_T}\dot{I}_T\right) + K_3 K_6\left(\dot{E}_{MT} - \frac{E_{MT}{}^*}{E_{MT}}\dot{E}_{MT}\right) \\
&+ K_3\sigma_{MT}\left(\dot{I}_{MT} - \frac{I_{MT}{}^*}{I_{MT}}\dot{I}_{MT}\right) + K_{11}\left(\dot{I}_V - \frac{I_V{}^*}{I_V}\dot{I}_V\right) + K_{12}\left(\dot{C} - \frac{C^*}{C}\dot{C}\right)
\end{aligned}
\tag{48}
$$

$$
\begin{aligned}
\dot{L} &= 2\lambda_2 S^* + 2\lambda_3 S^* + 2\mu_H S^* - \mu_H S - \frac{\lambda_2 (S^*)^2}{S} - \frac{\lambda_3 (S^*)^2}{S} - \frac{\mu (S^*)^2}{S} - \frac{\lambda_2 S E_M{}^*}{E_M} - \frac{\lambda_3 S E_T{}^*}{E_T} \\
&- \frac{\lambda_4 S E_{MT}{}^*}{E_{MT}} + K_1 E_M{}^* - \frac{K_1 E_M{}^* I_M}{I^*{}_M} - \frac{K_1 E_M I_M{}^*}{I_M} + K_1 E_M + K_2 E_T{}^* - \frac{K_2 E_T{}^* I_T}{I^*{}_T} - \frac{K_2 E_T I_T{}^*}{I_T} \\
&+ K_2 E_T + K_3 E_{MT}{}^* - \frac{K_3 E_{MT}{}^* I_{MT}}{I^*{}_{MT}} - \frac{K_3 E_{MT} I_{MT}{}^*}{I_{MT}} + K_3 E_{MT} - \mu_H R_M - \frac{\mu_H (R_M{}^*)^2}{R_M} + 2\mu_H R_M{}^* - \mu_H R_T \\
&- \frac{\mu_H (R_T{}^*)^2}{R_T} + 2\mu_H R_T{}^* - \mu_H R_{MT} - \frac{\mu_H (R_{MT}{}^*)^2}{R_{MT}} + 2\mu_H R_{MT}{}^* + 2\lambda_5 S_V{}^* + 2\mu_{Vi} S_V{}^* - \mu_{Vi} S_V - \frac{\lambda_5 (S_V{}^*)^2}{S_V} \\
&- \frac{\mu_{Vi} (S_V{}^*)^2}{S_V} - \frac{\lambda_5 S_V I_V{}^*}{I_V} + K_{11} I_V{}^* - \frac{K_{11} I_V{}^* C}{C^*} - \frac{K_{11} I_V C^*}{C} + K_{11} I_V - \mu_C C - \frac{\mu_C (C^*)^2}{C} + 2\mu_C C^*
\end{aligned}
\tag{49}
$$

Simplifying and factorizing Equation (49) using the AM–GM inequality to obtain the equation below;

$$
\begin{aligned}
\dot{L} &= \mu_H S^* \left(2 - \frac{S^*}{S} - \frac{S}{S^*}\right) + K_1 E_M{}^* \left(4 - \frac{S^*}{S} - \frac{E_M{}^*}{E_M} - \frac{I_M}{I_M{}^*} - \frac{I_M{}^*}{I_M}\right) + K_2 E_T{}^* \left(4 - \frac{S^*}{S} - \frac{E_T{}^*}{E_T} - \frac{I_T}{I_T{}^*} - \frac{I_T{}^*}{I_T}\right) \\
&+ K_3 E_{MT}{}^* \left(4 - \frac{S^*}{S} - \frac{E_{MT}{}^*}{E_{MT}} - \frac{I_{MT}}{I_{MT}{}^*} - \frac{I_{MT}{}^*}{I_{MT}}\right) + \mu_H R_M{}^* \left(2 - \frac{R_M{}^*}{R_M} - \frac{R_M}{R_M{}^*}\right) + \mu_H R_T{}^* \left(2 - \frac{R_T{}^*}{R_T} - \frac{R_T}{R_T{}^*}\right) \\
&+ \mu_H R_{MT}{}^* \left(2 - \frac{R_{MT}{}^*}{R_{MT}} - \frac{R_{MT}}{R_{MT}{}^*}\right) + \mu_{Vi} S_V{}^* \left(2 - \frac{S_V{}^*}{S_V} - \frac{S_V}{S_V{}^*}\right) + K_{11} I_V{}^* \left(4 - \frac{S_V{}^*}{S_V} - \frac{I_V{}^*}{I_V} - \frac{C}{C^*} - \frac{C^*}{C}\right) \\
&+ \mu_C C^* \left(2 - \frac{C^*}{C} - \frac{C}{C^*}\right)
\end{aligned}
\tag{50}
$$

Since the arithmetic mean is greater than the geometric mean, then

$$2-\frac{S^*}{S}-\frac{S}{S^*}\le 0,\qquad 4-\frac{S^*}{S}-\frac{E_M^{\ *}}{E_M}-\frac{I_M}{I_M^{\ *}}-\frac{I_M^{\ *}}{I_M}\le 0,$$

$$2-\frac{R_M^{\ *}}{R_M}-\frac{R_M}{R_M^{\ *}}\le 0,\qquad 4-\frac{S^*}{S}-\frac{E_T^{\ *}}{E_T}-\frac{I_T}{I_T^{\ *}}-\frac{I_T^{\ *}}{I_T}\le 0,$$

$$2-\frac{R_T^{\ *}}{R_T}-\frac{R_T}{R_T^{\ *}}\le 0,\qquad 4-\frac{S^*}{S}-\frac{E_{MT}^{\ *}}{E_{MT}}-\frac{I_{MT}}{I_{MT}^{\ *}}-\frac{I_{MT}^{\ *}}{I_{MT}}\le 0,$$

$$2-\frac{R_{MT}^{\ *}}{R_{MT}}-\frac{R_{MT}}{R_{MT}^{\ *}}\le 0,\qquad 4-\frac{S_V^{\ *}}{S_V}-\frac{I_V^{\ *}}{I_V}-\frac{C}{C^*}-\frac{C^*}{C}\le 0,$$

$$2-\frac{C^*}{C}-\frac{C}{C^*}\le 0$$

$$2-\frac{S_V^{\ *}}{S_V}-\frac{S_V}{S_V^{\ *}}\le 0,$$

Since all model parameters are positive, it follows that $L<0$. Hence, by the LaSalle Invariance Principle [17], every solution of the model converges to the endemic equilibrium ε^* as $t\to\infty$ whenever $R_0^{MT}>1$.

Theorem 3.7 implies that malaria-typhoid co-infection remains endemic in the community, independent of the initial population sizes, whenever $R_0^{MT}>1$.

3.3.4. *Sensitivity analysis of malaria-typhoid fever model*

In this section, sensitivity analysis is carried out to study the effect of parameter variations on the co-infection model outcomes, highlighting the most influential parameters and confirming the stability of the model results under uncertainty.

The normalized forward sensitivity index of R_{0M} with respect to a parameter w is defined as:

$$X_w^{R_0^{MT}}=\frac{\partial R_0^{MT}}{\partial w}\frac{w}{R_0^{MT}} \qquad (51)$$

The results obtained are presented in table 4 showing the indices of all parameters in R_{0M}

Table 5. Sensitivity indices quantifying the influence of co-infection model parameters on R_0^{MT}

Parameters	Sensitivity Expression	Value	Index
α	$-\left(\frac{\alpha}{1-\alpha}\right)$	-1	-
β_3	1	1	+

σ_{MT}	$\frac{\mu_H}{K_3}$	0.0341	+
γ_{MT}	$-\frac{\gamma_{MT}}{K_6}$	-0.66022	-
μ_H	$-\frac{(K_6)\mu_H + \mu_H + \sigma_{MT}}{K_3 K_6}$	-0.08821	-
δ_{IMT}	$-\frac{1}{2}\frac{\delta_{IMT}}{K_6}$	-0.00931	-

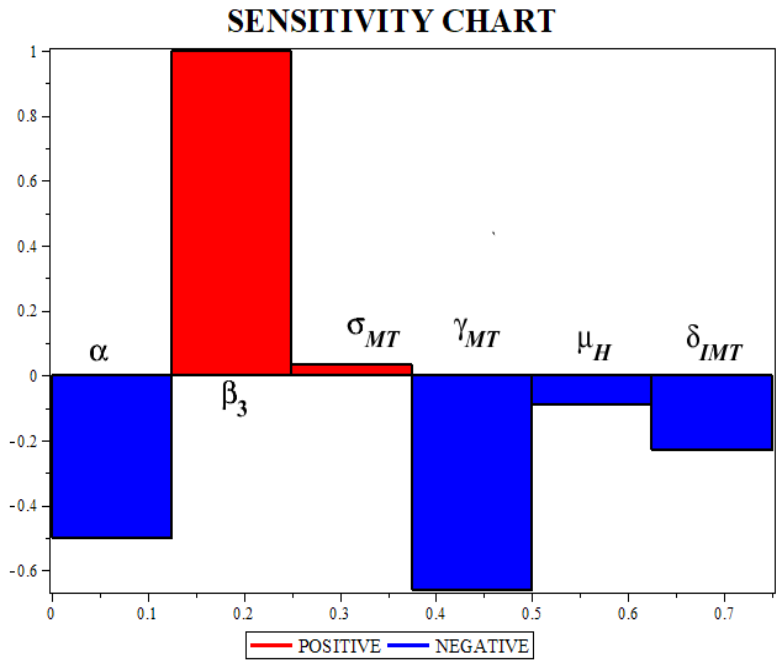


Figure 4: Bar chart showing the sensitivity indices of the effective reproduction number (R_{0MT}), indicating the relative influence of model parameters on malaria-typhoid co-infection transmission.

4.0 Numerical simulations

The analytical results established in the preceding chapters provide a rigorous theoretical foundation for understanding the transmission dynamics of malaria-typhoid co-infection. However, mathematical analysis alone, while essential, offers limited insight into the quantitative behavior of the system under realistic epidemiological conditions and varying intervention intensities. To complement the qualitative findings, this chapter presents a comprehensive set of numerical experiments designed to simulate the temporal evolution of all model compartments, assess the individual and combined impacts of control interventions, and visualize the sensitivity of disease outcomes to key epidemiological parameters.

The numerical simulations are carried out over a 365-day horizon using the fourth-order Runge–Kutta integration scheme, which provides sufficient accuracy and numerical stability for the nonlinear differential equation systems governing the full co-infection model, the malaria-only sub-model, and the typhoid-only sub-model. All simulations are initialized using biologically plausible starting conditions, with a total human population of 10,000 individuals distributed across susceptible, exposed, infectious, and recovered compartments, alongside mosquito vector populations and an initial environmental bacterial concentration reflective of an active typhoid outbreak setting. Parameter values are drawn from published epidemiological literature on malaria and typhoid transmission dynamics while parameters lacking direct empirical estimates are assigned reasonable assumed values consistent with the biological interpretation of the model.

The chapter is organized into three main sections corresponding to the full co-infection model, the malaria-only sub-model, and the typhoid-only sub-model respectively. Within each section, baseline dynamics are first presented to establish reference behavior in the absence of interventions, followed by sensitivity analyses examining how progressive increases in vaccination coverage, treatment rates, vector control intensity, environmental decontamination, and bacterial shedding reduction individually reshape disease trajectories. Together, these experiments provide actionable quantitative evidence to guide public health decision-making in regions where malaria and typhoid co-circulate.

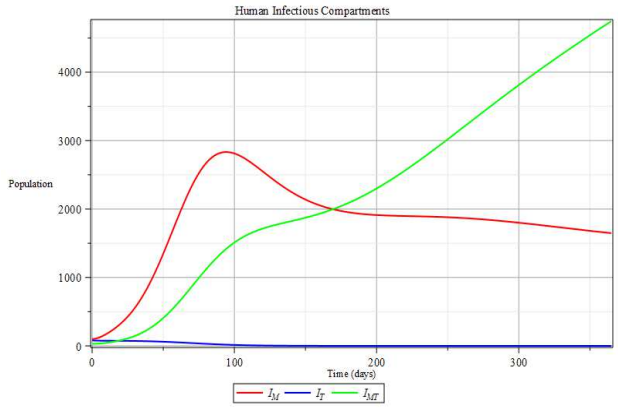


Figure 5Human Infectious Compartments **(I_M, I_T, I_{MT})**

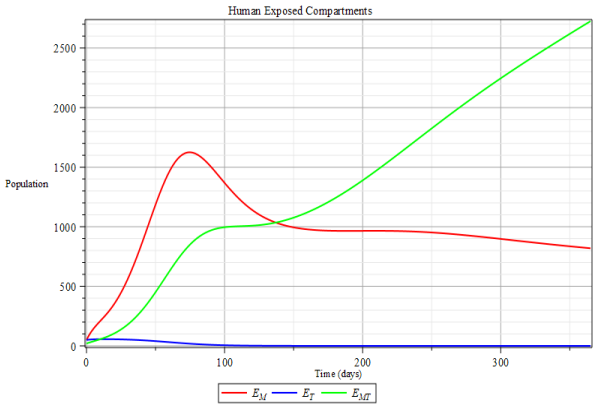


Figure 6: Human Exposed Compartments **(E_M, E_T, E_{MT})**

Figure 5 illustrates the temporal dynamics of the three human infectious compartments: malaria-only infected (I_M), typhoid-only infected (I_T), and co-infected (I_{MT}) individuals over a 365-day period. Initially, all three compartments begin at their respective starting values and evolve under the influence of the forces of infection driven by mosquito bites and environmental bacterial exposure. The malaria infectious class $I_M$rises sharply due to high mosquito-to-human transmission, while $I_T$starts low and declines steadily to near zero, because the environmental transmission pathway weakens as the bacterial concentration collapses (Figure 10). The co-infected compartment I_{MT}reflects simultaneous exposure to both pathogens. Over the 365-day

period, the malaria-only class I_M peaks at roughly 2,800 around day 95 and then declines slowly, whereas the co-infected class I_{MT} rises continuously, passing 4,500 by day 365 without reaching a steady state. This sustained growth stems from the demographic structure of the model: new individuals are recruited at the constant rate $\Lambda = 750$ per day, while natural mortality removes them at only $\mu_H = 0.0189$ per day. The corresponding carrying capacity of the total population, $\Lambda/\mu_H \approx 39{,}683$, is nearly four times the initial population of 10,000, so the population keeps expanding throughout the simulation and the infectious classes, I_{MT} in particular, have not yet reached an endemic equilibrium by day 365. These dynamics demonstrate the persistent and growing burden of both diseases in the absence of strong intervention measures.

Figure 6 depicts the dynamics of the exposed human compartments: individuals exposed to malaria only (E_M), typhoid only (E_T), and both pathogens simultaneously (E_{MT}) over 365 days. These compartments represent the latent period during which individuals have acquired infection but are not yet infectious to others. The exposed malaria class E_M rises quickly, reflecting the efficiency of mosquito-borne transmission, peaking at about 1,600 around day 75 before declining to about 800 by day 365, while E_T starts low and declines to near zero by about day 100, as the environmental transmission pathway weakens (Figure 10). The co-exposed class E_{MT} rises to about 1,000 by day 90, plateaus briefly, and then climbs steadily to about 2,700 by day 365, becoming the largest exposed class and indicating growing simultaneous exposure. As exposed individuals progress to the infectious stage at rates σ_M, σ_T, and σ_{MT} respectively, the malaria-only and typhoid-only compartments level off, reflecting a balance between new exposures and progression to active infection. The co-exposed class has not stabilized by day 365: as with the co-infected and recovered classes in Figures 5 and 7, its continued growth reflects the expanding total population under demographic recruitment (carrying capacity $\Lambda/\mu_H \approx 39{,}683$).

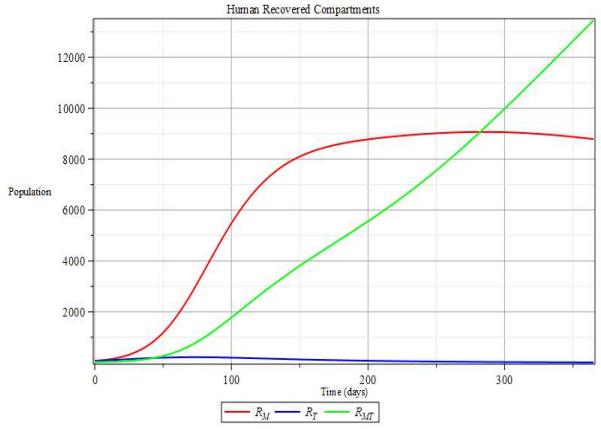


Figure 7: Human Recovered Compartments (R_M, R_T,R_{MT})

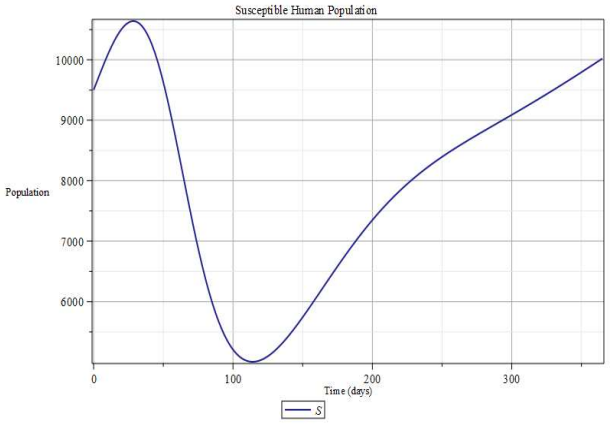


Figure 8: Susceptible Human Population (S)

Figure 7 presents the recovery dynamics of individuals who have cleared malaria (R_M), typhoid (R_T), or co-infection (R_{MT}) over 365 days. Recovery compartments accumulate as treatment rates γ_M, γ_T, and γ_{MT}remove individuals from their respective infectious classes. The malaria recovery class $R_M$grows most rapidly, consistent with the higher infectious malaria burden observed in

Figure 5. The typhoid recovery class $R_T$rises more slowly, reflecting lower treatment uptake and slower natural clearance. The co-infection recovery class R_{MT} grows more slowly at first but rises almost linearly, overtaking R_M at about day 280 and exceeding 13,000 by day 365, which is more than the initial total population of 10,000. This continued accumulation mirrors the unbounded growth of the co-infected class I_{MT} in Figure 5 and is explained by demographic recruitment: new individuals enter at the rate $\Lambda = 750$ per day, whereas natural mortality removes them at only $\mu_H = 0.0189$ per day, giving a carrying capacity of $\Lambda/\mu_H \approx 39{,}683$. The total population therefore grows well beyond 10,000 over the 365-day window, and the recovered classes can legitimately exceed the initial population size. Importantly, recovered individuals are not permanently immune; waning immunity at rates ω_M, ω_T, and ω_{MT}returns them to the susceptible class, sustaining long-term disease circulation.

Figure 8 tracks the dynamics of the susceptible human population Sover 365 days. Initially set at 9,500 individuals, the susceptible class first rises to about 10,600 around day 30, because recruitment outpaces early losses, and then declines as individuals become exposed to malaria through infected mosquito bites, to typhoid through environmental bacterial contamination, and to co-infection through simultaneous exposure. The rate of decline is governed by the combined force of infection $\lambda_1 + \lambda_2 + \lambda_3$acting on susceptibles. Over time, as recovered individuals return to the susceptible pool through waning immunity at rates ω_M, ω_T, and ω_{MT}, and as new individuals enter through recruitment Λ, the susceptible class reaches a minimum of about 5,000 near day 115 and then recovers steadily, reaching roughly 10,000 by day 365 while still rising rather than settling at an equilibrium; this continued increase reflects the growing total population discussed for Figures 5 and 7. This figure highlights how susceptibility is continuously replenished, sustaining ongoing transmission in the population.

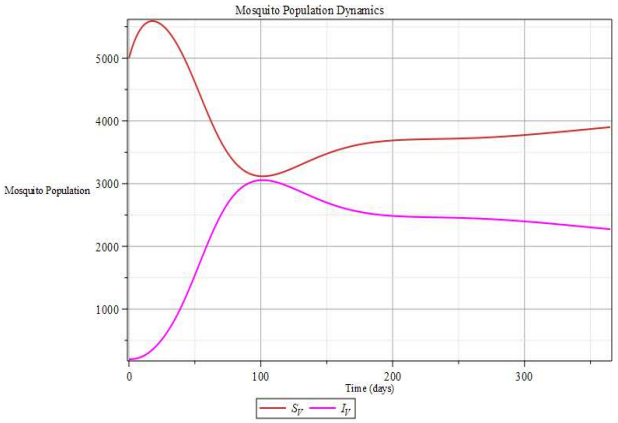


Figure 9: Mosquito Population Dynamics (S_V, I_V)

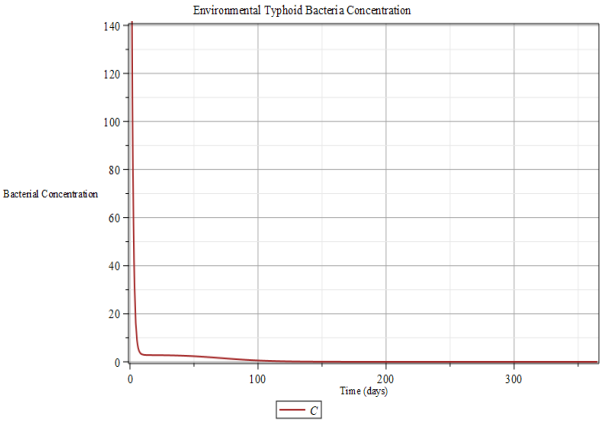


Figure 10: Environmental Typhoid Bacteria Concentration (C)

Figure 9 illustrates the dynamics of the mosquito vector population, distinguishing between susceptible mosquitoes (S_V) and infected mosquitoes (I_V) over 365 days. The susceptible mosquito population begins at 5,000 and declines as mosquitoes acquire malaria parasites through biting malaria-infectious humans at rate $\beta_V b$. Simultaneously, the infected mosquito compartment $I_V$rises initially as parasite acquisition outpaces mosquito mortality, before

stabilizing at an endemic level governed by the balance between new infections and mosquito death rates μ_{Vs}, μ_{Vi}, and control rates ϕ_{Vs}, ϕ_{Vi}. The infected mosquito population is the primary driver of malaria transmission to humans through λ_1, making vector control a critical intervention target for reducing overall disease burden.

Figure 10 shows the temporal evolution of typhoid bacteria concentration Cin the environment over 365 days. Bacteria enter the environment through shedding by typhoid-infectious individuals I_T at rate ρ_T, and are removed through natural bacterial death at rate $\mu_C$and environmental decontamination at rate θ. Starting at an initial concentration of 500 units, the bacterial load falls sharply within the first 10 days, as natural die-off and environmental decontamination remove bacteria much faster than the small typhoid-infectious population can replenish them through shedding. The concentration then remains very close to zero and essentially flat for the rest of the simulation, indicating that shedding by the typhoid-infectious class is too small to sustain a substantial environmental reservoir under baseline conditions. The level of C directly determines the magnitude of the waterborne / food borne force of infection λ_2, making sanitation and disinfectants essential control tools.

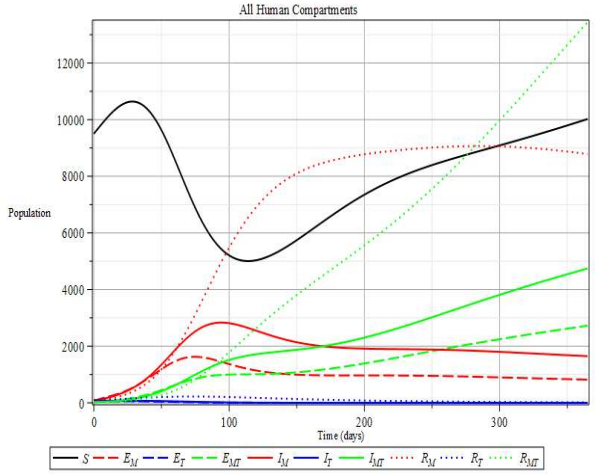


Figure 11: All Human Compartments

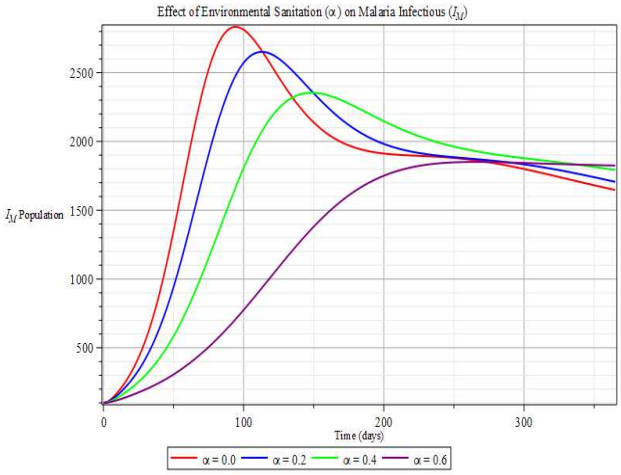
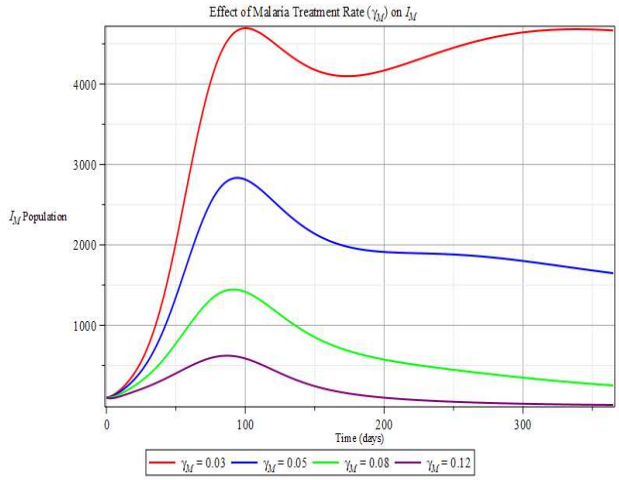


Figure 12: Effect of Environmental Sanitation (α) on I_M

Figure 11 provides a comprehensive overview of all ten human compartments simultaneously over 365 days, distinguishing between susceptible (S), exposed (E_M, E_T, E_{MT}), infectious (I_M, I_T, I_{MT}), and recovered (R_M, R_T, R_{MT}) individuals. Different line styles are used to distinguish compartment categories: solid lines for susceptible and infectious classes, dashed lines for exposed classes, and dotted lines for recovered classes. The figure reveals the hierarchical structure of the epidemic, with the susceptible class dominating numerically, followed by the recovered classes as treatment effects accumulate. The infectious and exposed classes remain comparatively smaller but persist at endemic levels. This consolidated view underscores the interconnected nature of all compartments and the overall epidemic trajectory of the co-infection system.

Figure 12 examines the sensitivity of the malaria infectious compartment I_M to varying levels of sanitation and personal protection coverage α over 365 days. Four values are tested: α = 0.0, 0.2,

0.4, and 0.6, representing no sanitation, moderate, and high coverage respectively. As α increases, the force of infection acting on susceptible and vaccinated individuals is proportionally reduced by the factor $(1-\alpha)$, directly lowering new malaria exposures. The results demonstrate that higher sanitation coverage produces progressively lower peaks and endemic levels of I_M. Even moderate sanitation at $\alpha = 0.2$yields a meaningful reduction, while $\alpha = 0.6$substantially suppresses malaria transmission, highlighting vaccination as one of the most impactful single interventions available against malaria in this co-infection framework.



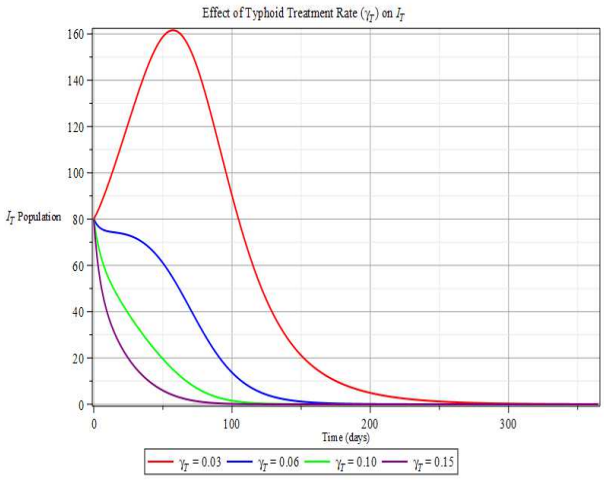


Figure 13: Effect of Malaria Treatment Rate (γ_M) on I_MFigure 14: Effect of Typhoid Treatment Rate (γ_T) on I_T

Figure 13 investigates the impact of varying malaria treatment rates γ_M on the infectious malaria compartment I_M over 365 days. Four treatment rates are evaluated: $\gamma_M = 0.03$, 0.05, 0.08, and 0.12per day, representing low to high therapeutic intervention intensity. As γ_M increases, infected malaria individuals are removed from I_M at faster rates and channelled into the recovery class R_M, reducing the overall infectious burden. The simulations show that higher treatment rates produce lower peak and equilibrium values of I_M, with $\gamma_M = 0.12$ achieving the most substantial suppression. This figure demonstrates that improving treatment access, drug efficacy, and healthcare coverage are critical strategies for reducing malaria transmission intensity and its contribution to co-infection dynamics.

Figure 14 explores the sensitivity of the typhoid infectious compartment I_T to varying typhoid treatment rates γ_T over 365 days. Four values are tested: $\gamma_T = 0.03$, 0.06, 0.10, and 0.15per day. Increasing γ_T accelerates the removal of typhoid-infected individuals into the recovered class R_T, while simultaneously reducing bacterial shedding into the environment since fewer infectious individuals remain active for longer durations. Higher treatment rates produce markedly lower I_T peaks and endemic levels. Notably, typhoid treatment also indirectly reduces environmental bacterial concentration C through the $\rho_T I_T$ term, thereby lowering the waterborne force of infection $\lambda_2$and reducing new typhoid and co-infection exposures. This underscores the dual benefit of aggressive typhoid treatment on both direct and environmental transmission pathways.

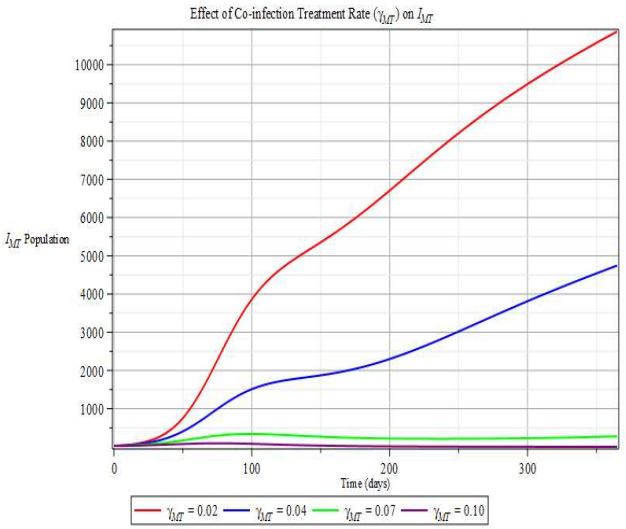


Figure 15: Co-infection Treatment Rate (γ_{MT}) on I_{MT}

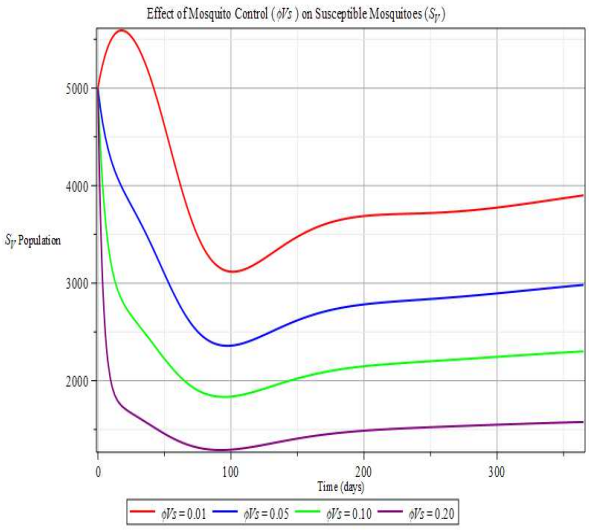


Figure 16: Mosquito Control (ϕ_{Vs}) on Sus. Mosquitoes S_V

Figure 15 assesses the impact of co-infection treatment rate γ_{MT} on the co-infected compartment I_{MT} over 365 days, testing four values: $\gamma_{MT} = 0.02$, 0.04, 0.07, and 0.10per day. Co-infected individuals face the highest disease burden as they simultaneously carry both malaria parasites and typhoid bacteria, making treatment of this group particularly challenging and critical. As γ_{MT} increases, co-infected individuals recover faster into R_{MT}, reducing the pool available to sustain co-infection transmission through λ_3. Higher treatment rates produce progressively lower I_{MT} peaks and endemic levels. Since co-infected individuals also contribute to both mosquito infection and environmental bacterial load, reducing I_{MT} through treatment has a cascading beneficial effect across the entire model system.

Figure 16 illustrates the effect of increasing the control rate of susceptible mosquitoes ϕ_{Vs} on the susceptible mosquito population S_V over 365 days. Four control intensities are evaluated: $\phi_{Vs} = 0.01$, 0.05, 0.10, and 0.20per day, representing escalating vector control efforts such as insecticide spraying, larval source reduction, and environmental management. As ϕ_{Vs} increases, susceptible mosquitoes are eliminated at higher rates, causing S_V to decline to progressively lower equilibrium levels. Reducing the susceptible mosquito pool directly limits the number of mosquitoes available to acquire malaria parasites from infectious humans, thereby constraining the growth of the infected mosquito compartment I_V and consequently reducing the force of infection $\lambda_1$on the human population.

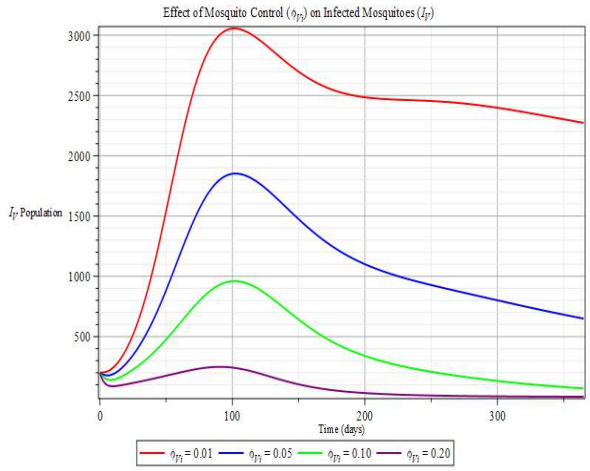


Figure 17: Mosquito Control (ϕ_{Vi}) on Infected Mosquitoes I_V

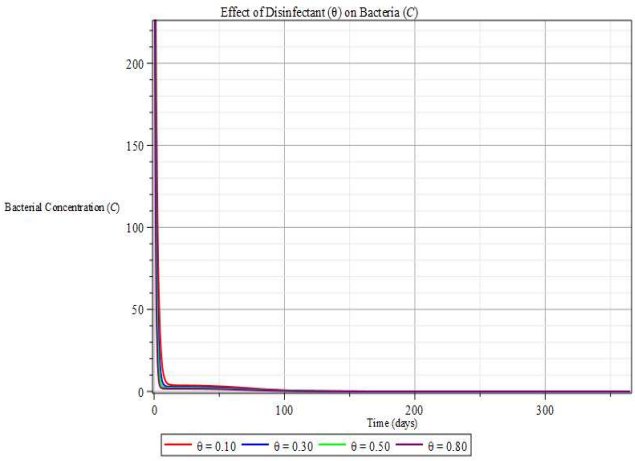
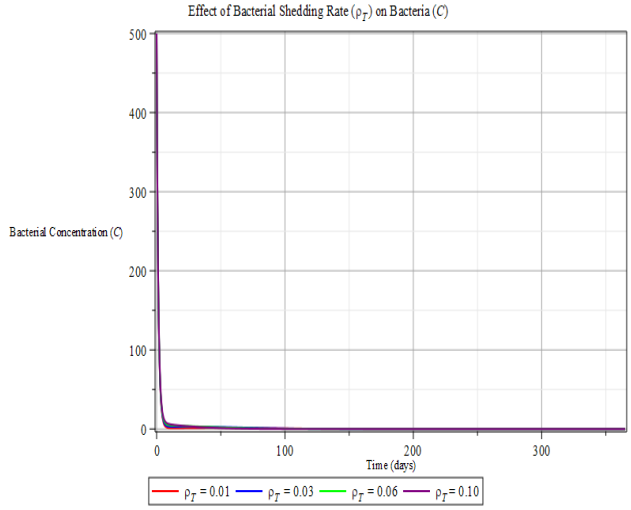


Figure 18: Effect of Disinfectant Rate (θ) on C

Figure 17 examines the sensitivity of the infected mosquito compartment I_V to varying infected mosquito control rates cover 365 days, with values ϕ_{Vi} = 0.01, 0.05, 0.10, and 0.20 per day. This control parameter represents interventions targeting adult infected mosquitoes, including indoor residual spraying, pyrethroid-treated nets, and targeted adulticide applications. Increasing ϕ_{Vi}directly accelerates the removal of malaria-infectious mosquitoes from the vector population, resulting in substantially lower I_V levels at both peak and equilibrium. Since the human malaria force of infection $\lambda_1 = \beta_h a I_V / N_H$, reducing I_V proportionally reduces new malaria exposures in the human population, demonstrating that killing infected mosquitoes is one of the most direct and effective strategies for malaria control.

Figure 18 demonstrates the impact of increasing the disinfectant rate on the typhoid bacterial concentration Cover 365 days, testing values $\theta = 0.10$, 0.30, 0.50, and 0.80per day. This parameter represents water treatment, chlorination, improved sewage disposal, food safety enforcement, and community hygiene interventions. As θ increases, the combined bacterial removal rate $\mu_C + \theta$ rises significantly, causing the environmental bacterial load to decline more rapidly and stabilize at much lower endemic concentrations. Lower bacterial concentration C directly reduces the waterborne force of infection λ_2, which drives typhoid exposure in the susceptible population. This figure strongly supports investment in water, sanitation, and hygiene infrastructure as a foundational typhoid control strategy.



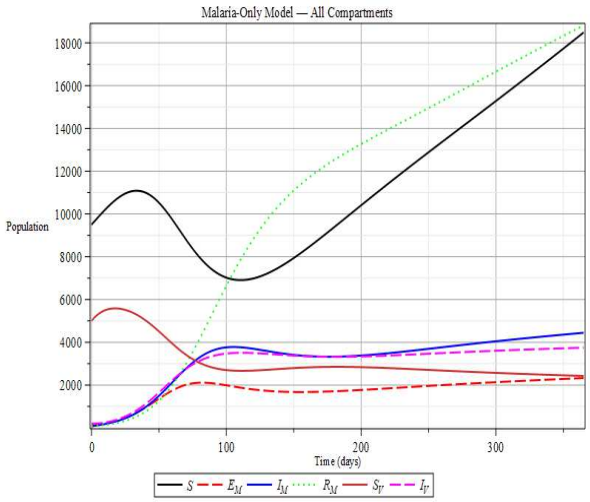
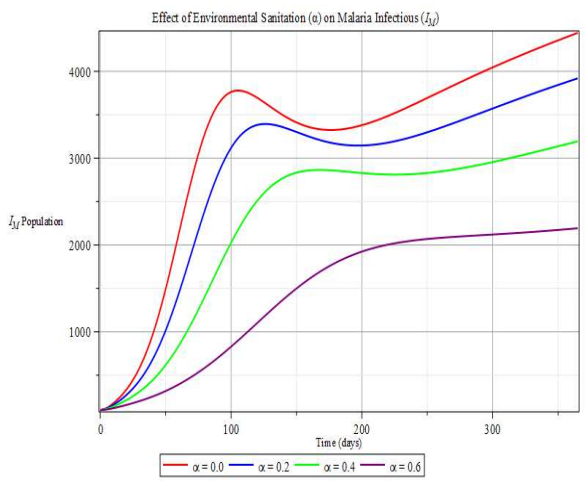


Figure 19: Effect of Bacterial Shedding Rate (ρ_T) on Bacterial Concentration Figure 20: Malaria-Only Model

Figure 19 investigates the influence of the typhoid bacterial shedding rate ρ_T on environmental bacterial concentration Cover 365 days, testing values $\rho_T = 0.01$, 0.03, 0.06, and 0.10per day. This parameter captures the rate at which typhoid-infected individuals deposit bacteria into water sources, food supplies, and the broader environment through inadequate sanitation. In Figure 19, all four curves start at the initial concentration of 500 units and fall rapidly to near zero within the first days of the simulation, after which they remain close to zero and are almost indistinguishable from one another. A higher shedding rate enlarges the source term and therefore tends to raise the bacterial concentration, amplifying the waterborne force of infection $\lambda_2$and driving more typhoid and co-infection exposures; over the tested range, however, this effect is barely visible in the full model because natural die-off and disinfection remove bacteria far faster than infectious individuals shed them. Conversely, reducing ρ_T through early treatment, patient isolation, and improved sanitation infrastructure keeps environmental bacterial loads low. Under these baseline conditions the bacterial concentration is governed mainly by natural die-off and disinfection, so reducing the source of contamination through behavioral and structural sanitation interventions acts as a complementary measure alongside treatment and disinfectant efforts.

Figure 20 presents a comprehensive overview of all six compartments of the malaria-only sub-model simultaneously over a 365-day simulation period. The compartments displayed include susceptible humans (S), exposed humans (E_M), infectious humans (I_M), recovered humans (R_M), susceptible mosquitoes (S_V), and infected mosquitoes (I_V). The susceptible human population dominates numerically and declines gradually as individuals are exposed through infectious mosquito bites governed by the force of infection $\lambda_H = (1 - \alpha)\beta_1 a I_V / N_H$. The mosquito compartments demonstrate rapid dynamics relative to humans due to shorter mosquito lifespans. All compartments eventually stabilize at endemic equilibrium levels, reflecting the persistent nature of malaria transmission in the absence of sufficiently strong intervention measures to drive the control reproduction number below unity.



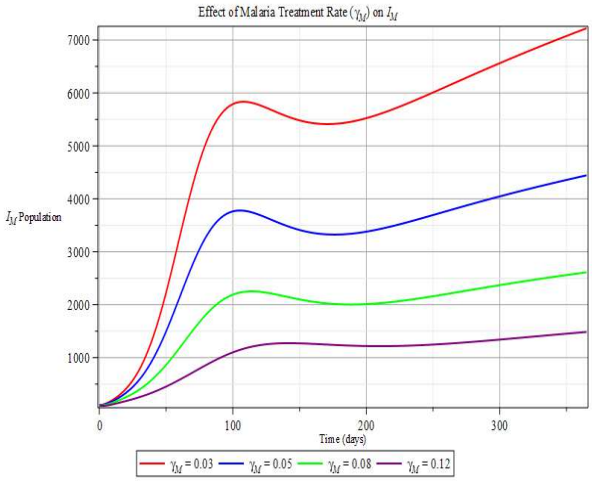


Figure 21: Effect of Environmental Sanitation (α) on I_M Figure 22: Effect of Malaria Treatment Rate (γ_M) on I_M

Figure 21 investigates the sensitivity of the malaria infectious compartment I_M to varying levels of sanitation α over 365 days in the malaria-only sub-model. Four sanitation levels are tested: $\alpha = 0.0$, 0.2, 0.4, and 0.6, representing no sanitation through to high coverage. The parameter α reduces the effective force of infection on susceptible humans by the multiplicative factor $(1 - \alpha)$, directly lowering new malaria exposures. Results demonstrate that even moderate protection at $\alpha = 0.2$ produces a meaningful reduction in peak and endemic I_M levels, while $\alpha = 0.6$achieves substantial suppression. This figure confirms that sanitation campaigns and personal protective measures such as insecticide-treated bed nets represent among the most impactful single interventions available for malaria control.

Figure 22 examines the impact of varying malaria treatment rates γ_M on the infectious malaria compartment I_M over 365 days. Four treatment intensities are evaluated: $\gamma_M = 0.03$, 0.05, 0.08, and 0.12per day, corresponding to the composite removal rate $K_4 = \gamma_M + \mu_H + \delta_{IM}$. As γ_M increases, infected individuals are removed from I_M more rapidly and channeled into the recovered class R_M, reducing the overall infectious burden available to infect susceptible mosquitoes. Higher treatment rates produce progressively lower peak and equilibrium I_M values, with $\gamma_M = 0.12$achieving the greatest suppression. This figure highlights that improving antimalarial drug access, treatment adherence, and healthcare coverage are essential strategies for reducing malaria transmission intensity within the population.

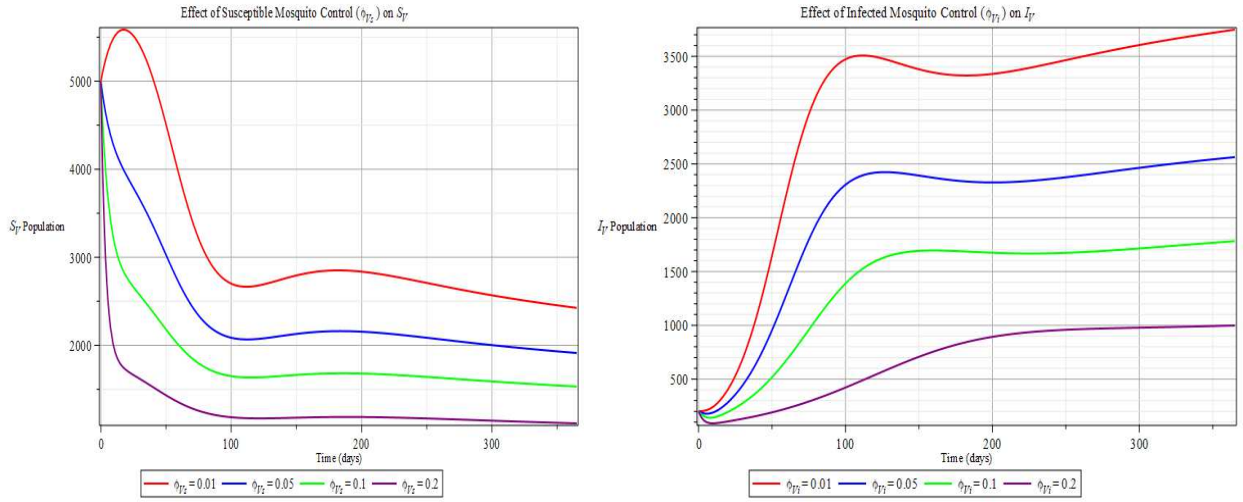


Figure 23: Susceptible Mosquito Control (ϕ_{Vs}) on S_V Figure 24: Infected Mosquito Control (ϕ_{Vi}) on I_V

Figure 23 demonstrates the effect of increasing the susceptible mosquito control rate ϕ_{Vs}on the susceptible mosquito population S_V over 365 days, testing four values: ϕ_{Vs} = 0.01, 0.05, 0.10, and 0.20per day. This parameter enters the composite term $K_{10} = \mu_{Vs} + \phi_{Vs}$, representing the combined removal rate of susceptible mosquitoes through natural death and active vector control interventions such as larval source reduction, indoor residual spraying, and environmental management. As ϕ_{Vs} increases, susceptible mosquitoes are eliminated at higher rates, driving $S_V$to progressively lower endemic equilibria. Reducing the susceptible mosquito pool directly constrains the number of vectors available to acquire malaria parasites from infectious humans, thereby limiting infected mosquito production and subsequently reducing human malaria exposure.

Figure 24 examines the sensitivity of the infected mosquito compartment I_V to varying infected mosquito control rates ϕ_{Vi} over 365 days, with values ϕ_{Vi} = 0.01, 0.05, 0.10, and 0.20per day. This parameter contributes to the composite removal rate $K_{11} = \mu_{Vi} + \phi_{Vi}$, representing natural mosquito mortality combined with targeted interventions that eliminate malaria-carrying adult mosquitoes, including indoor residual spraying with long-lasting insecticides, pyrethroid-treated bed nets, and targeted adulticide applications. Increasing ϕ_{Vi} directly accelerates removal of infectious mosquitoes, producing substantially lower I_V levels at both peak and endemic equilibrium. Since the human malaria force of infection $\lambda_H = (1 - \alpha)\beta_1 a I_V / N_H$ scales directly with I_V, reducing infected mosquitoes proportionally suppresses new human malaria infections throughout the simulation period.

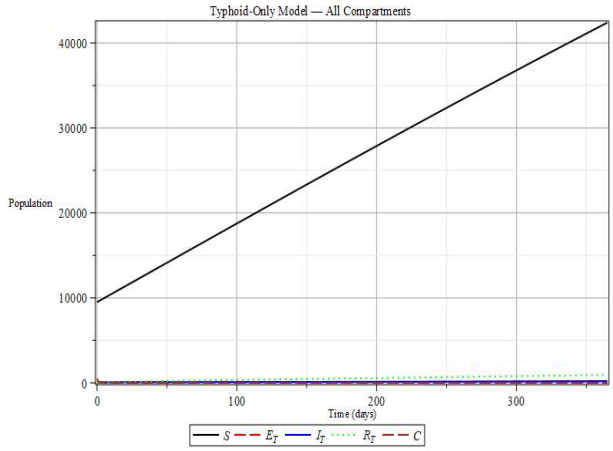


Figure 25: Typhoid-Only Model

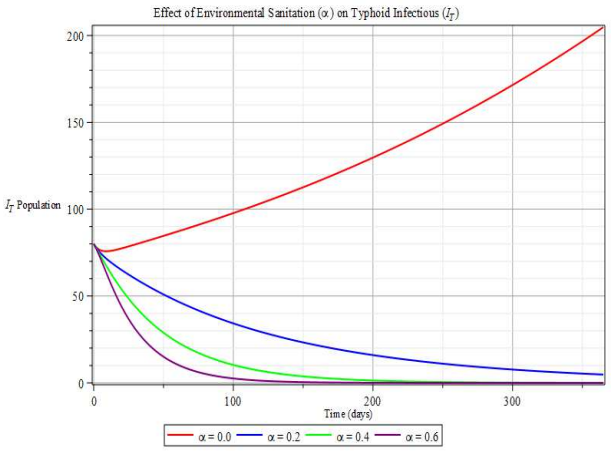


Figure 26: Environmental Sanitation (α) on I_T

Figure 25 presents a comprehensive overview of all five compartments of the typhoid-only sub-model simultaneously over a 365-day simulation period. The compartments displayed include susceptible humans (S), exposed humans (E_T), infectious humans (I_T), recovered humans (R_T), and environmental bacterial concentration (C). Susceptible individuals acquire typhoid infection through contact with contaminated environments at force of infection $\lambda_T = (1 - \alpha)\beta_2 k I_T / N_H$. Exposed individuals progress to the infectious class at progression rate σ_T after the incubation period defined by composite parameter K_2. The bacterial concentration C accumulates through shedding by infectious individuals at rate ρ_T and declines through natural die-off and decontamination at combined rate K_{12}. All compartments stabilize at endemic equilibrium, reflecting persistent typhoid circulation under baseline parameter conditions.

Figure 26 investigates the sensitivity of the typhoid infectious compartment I_T to varying levels of sanitation and personal hygiene protection coverage α over 365 days. Four sanitation levels are tested: $\alpha = 0.0$, 0.2, 0.4, and 0.6, representing no sanitation through progressively higher intervention coverage. The parameter α enters the model through the reduced force of infection $(1 - \alpha)\beta_2 k I_T / N_H$, directly lowering the rate at which susceptible individuals acquire typhoid infection. Results clearly demonstrate that increasing α produces progressively lower peak and endemic I_T levels. Even moderate protection at $\alpha = 0.2$yields meaningful reductions, while $\alpha = 0.6$achieves substantial suppression of typhoid transmission. This underscores sanitation, clean water access, and personal hygiene promotion as critical typhoid prevention strategies.

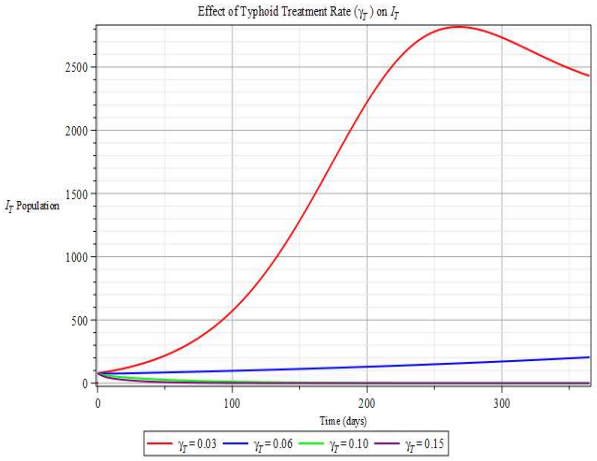


Figure 27: Effect of Typhoid Treatment Rate (γ_T) on I_T

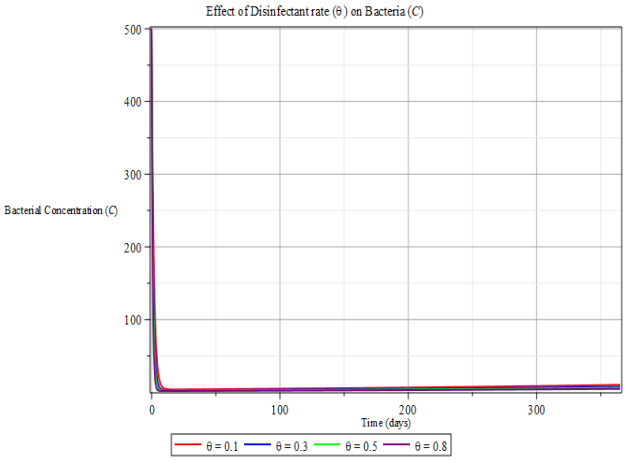


Figure 28: Effect of Disinfectant Rate (θ) on C

Figure 27 examines the impact of varying typhoid treatment rates γ_T on the infectious typhoid compartment I_T over 365 days. Four treatment intensities are evaluated: $\gamma_T = 0.03$, 0.06, 0.10, and 0.15per day, representing low to high therapeutic coverage through antibiotic administration. Increasing γ_T raises the composite removal rate $K_5 = \gamma_T + \mu_H + \delta_{IT}$, accelerating the clearance of infectious individuals from I_T into the recovered class R_T. Higher treatment rates produce markedly lower peak and endemic I_T values across all simulations. Importantly, faster recovery also reduces the duration of bacterial shedding per individual, indirectly lowering environmental bacterial concentration C and subsequently reducing the waterborne force of infection λ_T acting on the susceptible population.

Figure 28 demonstrates the impact of increasing the disinfectant rate θ on typhoid bacterial concentration Cover 365 days, testing four values: $\theta = 0.10$, 0.30, 0.50, and 0.80per day. This parameter enters the composite bacterial removal rate $K_{12} = \mu_C + \theta$, representing active interventions that eliminate bacteria from water sources and the environment, including chlorination, water treatment, improved sewage disposal, food safety enforcement, and community hygiene campaigns. As θ increases, bacterial concentration declines more rapidly and stabilizes at substantially lower endemic equilibrium levels. Since C directly drives the waterborne force of infection λ_T, maintaining high disinfectant rates fundamentally suppresses new typhoid exposures and represents one of the most impactful structural interventions available for typhoid elimination.

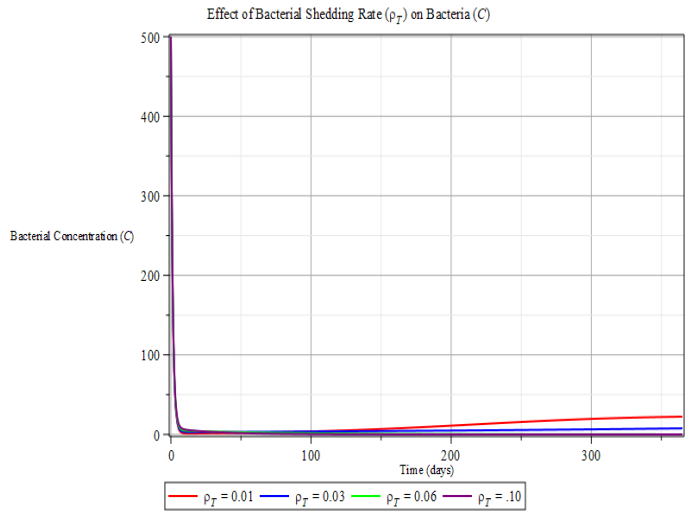


Figure 29: Effect of Bacterial Shedding Rate (ρ_T) on C

Figure 29 investigates the influence of the typhoid bacterial shedding rate ρ_T on environmental bacterial concentration Cover 365 days, evaluating four values: $\rho_T = 0.01$, 0.03, 0.06, and 0.10per day. This parameter acts solely as a source term $\rho_T I_T$ in the bacterial equation, governing how rapidly infectious individuals contaminate the environment. It does not enter the composite infectious removal rate $K_5 = \gamma_T + \mu_H + \delta_{IT}$, because shedding bacteria into the environment does not remove a patient from the infectious human compartment; that removal depends only on treatment, natural mortality, and disease-induced death. Higher shedding rates therefore produce greater bacterial concentrations, amplifying λ_T and driving more new typhoid infections. Reducing ρ_T through early treatment, patient isolation, improved toilet facilities, and hand-washing infrastructure simultaneously lowers environmental contamination and suppresses ongoing typhoid transmission throughout the population.

Summary, Findings, Conclusion, and Recommendations

5.0 Summary, Conclusion and Recommendation

This chapter presents a comprehensive suite of numerical experiments designed to complement the analytical results derived for the malaria–typhoid co-infection model. Because closed-form mathematical analysis offers limited insight into the quantitative, time-dependent behavior of a nonlinear compartmental system, the numerical experiments simulate the full co-infection model together with its two constituent sub-models, a malaria-only model and a typhoid-only model,over a 365-day horizon.

Simulations were carried out using the fourth-order Runge–Kutta integration scheme, chosen for its accuracy and stability when solving the coupled nonlinear differential equations governing human, mosquito, and environmental bacterial compartments. All experiments were initialized from biologically plausible starting conditions representing a population of $N(0) = 10{,}000$ individuals distributed across susceptible, exposed, infectious, and recovered classes, together with an active mosquito vector population and an environmental bacterial load consistent with an ongoing typhoid outbreak. Parameter values were drawn primarily from published

epidemiological literature with unmeasured parameters assigned biologically reasonable assumed values.

The chapter is organized into three parts: (i) baseline and sensitivity dynamics of the full co-infection model, (ii) baseline and sensitivity dynamics of the malaria-only sub-model, and (iii) baseline and sensitivity dynamics of the typhoid-only sub-model. Within each part, the disease-free/baseline trajectory is first established, after which key control parameters — sanitation/personal-protection coverage, disease-specific treatment rates, vector control intensity, environmental disinfection, and bacterial shedding, are varied individually to assess their influence on infection burden.

Key Findings

Baseline (No-Intervention) Dynamics

In the absence of interventions, all human, vector, and bacterial compartments in the full co-infection model persist rather than dying out, although the co-infected and recovered classes are still growing at the end of the 365-day horizon rather than reaching a steady state. This growth arises because recruitment (Λ = 750 per day) greatly exceeds natural mortality (μ_H = 0.0189 per day), so the total population expands toward a carrying capacity of $\Lambda/\mu_H \approx$ 39,683. The malaria-only infectious class $I_M(t)$rises sharply, reflecting efficient mosquito-borne transmission, while the typhoid-only class $I_T(t)$ grows more gradually through the slower environmental (waterborne/foodborne) pathway. The co-infected class $I_{MT}(t)$ remains smaller but persistently nonzero, confirming that individuals are simultaneously vulnerable to both pathogens. Recovered individuals do not remain permanently immune: waning immunity steadily returns them to the susceptible pool, which combined with new recruitment, sustains long-term transmission. Mosquito populations stabilize quickly given their short lifespan, and the environmental bacterial concentration $C(t)$falls rapidly from its initial value to a level close to zero, where it remains because natural decay and disinfection remove bacteria much faster than infectious individuals shed them.

Effect of Sanitation and Personal Protection (α)

Across all three models (full, malaria-only, typhoid-only), increasing the sanitation/personal-protection coverage parameter α = 0.0, 0.2, 0.4, 6produced consistent and substantial reductions in infectious peaks and endemic levels for both malaria (I_M) and typhoid (I_T). Because αscales down the force of infection multiplicatively, even moderate coverage (α = 0.2) yielded meaningful gains, while high coverage (α = 0.6) achieved strong suppression of transmission in every scenario tested. This makes αone of the single most impactful levers in the model.

Effect of Disease Specific Treatment Rates (γ_M, γ_T, γ_{MT})

Raising the malaria treatment rate $\gamma_M = [0.03, 0.12]$ day^{-1}consistently lowered both the peak and endemic level of $I_M$by accelerating movement of infectious individuals into recovery. The same pattern held for the typhoid treatment rate $\gamma_T = [0.03, 0.15]$day^{-1}on I_T, with the added benefit that faster typhoid recovery shortens the duration of bacterial shedding, indirectly lowering the environmental bacterial load and the resulting waterborne force of infection. Increasing the co-infection treatment rate $\gamma_{MT} = [0.02, 0.10]$ day^{-1}produced the same suppressive effect on $I_{MT}$and, because co-infected individuals also seed mosquito infection and environmental contamination, generated cascading benefits across the rest of the system.

Effect of Mosquito Vector Control (ϕ_{Vs}, ϕ_{Vi})

Increasing the control rate applied to susceptible mosquitoes $\phi_{Vs} = [0.01, 0.20]$ day^{-1}reduced the size of the susceptible vector pool available to acquire malaria parasites, indirectly constraining growth of the infected mosquito compartment. Increasing the control rate applied to infected mosquitoes $\phi_{Vi} = [0.01, 0.20]$ day^{-1}had an even more direct effect, substantially lowering both peak and endemic infected-mosquito levels and, through the force of infection, producing a proportional reduction in new human malaria cases. Vector control targeting infectious mosquitoes therefore emerged as one of the most direct and effective single-parameter interventions against malaria transmission.

Effect of Environmental Disinfection (θ) and Bacterial Shedding (ρ_T)

Increasing the environmental disinfectant rate $\theta = [0.10, 0.80]$ day^{-1}raised the combined bacterial removal rate, causing environmental bacterial concentration $C(t)$to decline more rapidly and stabilize at much lower endemic levels ,directly suppressing the waterborne force of infection driving typhoid exposure. Conversely, higher bacterial shedding rates $\rho_T = [0.01, 0.10]$ day^{-1}enlarge the bacterial source term and therefore tend to raise bacterial concentration and amplify new typhoid and co-infection exposures, although over the tested range the differences in bacterial concentration were small because it decays rapidly to near zero. These results confirm that water, sanitation, and hygiene (WASH) infrastructure and reducing the rate at which infectious individuals contaminate the environment through early isolation and treatment is as important as clinical treatment for typhoid control.

Consistency Across Sub-models

The malaria-only and typhoid-only sub-models reproduced, in isolation, the same qualitative sensitivity patterns observed in the full co-infection model: sanitation/protection coverage, disease-specific treatment, vector control, and environmental disinfection each independently suppressed their respective infectious compartments. This consistency indicates that the full model's behavior is not an artifact of coupling but reflects robust, mechanistically grounded transmission dynamics, and that single-disease interventions retain their effectiveness even when malaria and typhoid co-circulate.

5.2 Conclusion

The numerical experiments confirm that, under baseline (no-intervention) conditions, malaria, typhoid, and malaria–typhoid co-infection all persist within the population, driven by the continuous replenishment of susceptibles through waning immunity and new recruitment; because recruitment exceeds natural mortality, the total population and the co-infected and recovered classes continue to grow over the 365-day horizon rather than settling at a steady state. No single compartment naturally declines to zero without sustained external intervention, underscoring the chronic public health burden posed by co-circulating vector-borne and environmentally transmitted diseases.

Across every scenario tested, the simulations demonstrate that disease burden is highly responsive to control effort: increased sanitation/personal-protection coverage, faster clinical treatment, more intensive mosquito vector control, and stronger environmental disinfection each independently and substantially reduce infectious peaks and endemic prevalence. Because co-infected individuals contribute simultaneously to mosquito infection and environmental contamination, interventions that reduce co-infection prevalence generate benefits that extend beyond the co-infected compartment itself. Taken together, the results validate the theoretical model as a credible quantitative tool for evaluating intervention strategies and provide strong numerical evidence that coordinated, multi-pronged control is more effective than reliance on any single measure.

5.3 Recommendations

Based on the findings of the numerical experiments, the following recommendations are proposed for public health planning in settings where malaria and typhoid co-circulate:

• Prioritize sanitation and personal protection (α): Scale up insecticide-treated bed nets, indoor residual spraying, safe water access, and hygiene promotion, since even moderate coverage produced meaningful reductions in both malaria and typhoid burden.

• Strengthen treatment access and adherence: Invest in expanding antimalarial and antibiotic treatment coverage, particularly for co-infected patients, given the disproportionately large downstream benefits of raising γ_{MT}.

• Intensify vector control targeting infectious mosquitoes: Direct resources toward adulticide spraying and other interventions that raise ϕ_{Vi}, which produced the most direct reductions in human malaria exposure among the vector-control parameters tested.

• Invest in WASH infrastructure and environmental disinfection: Support chlorination, improved sewage disposal, and food safety enforcement to raise θ, and pair this with early isolation/treatment of typhoid cases to reduce bacterial shedding (ρ_T) at its source.

• Adopt integrated, multi-intervention strategies: Because each control measure acts through a different transmission pathway, combining sanitation, treatment, vector control, and disinfection

is likely to outperform any single intervention, particularly for suppressing the co-infected compartment.

• Use the model to guide resource allocation: Given the demonstrated sensitivity of outcomes to specific parameters, decision-makers should use model-based simulations of this kind to prioritize interventions where local data indicate the greatest marginal impact per unit cost.

• Extend future work: Subsequent studies should incorporate cost-effectiveness analysis, optimal control theory, and validation against field surveillance data to translate these numerical insights into concrete, budget-constrained intervention plans.

References

1] T. A. Olowolafe, O. F. Agosile, A. O. Akinpelu, N. Aderinto, O. Z. Wada, and D. B. Olawade, "Malaria and typhoid fever co-infection: A retrospective analysis of University Hospital records in Nigeria," Malaria Journal, vol. 23, Art. no. 220, 2024. DOI: https://doi.org/10.1186/s12936-024-05052-4.

[2] N. Y. Shehu, J. Bimba, D. Nantok, I. Kelly, O. Obrerhor, S. S. Gomerep, and K. I. Onyedibe, "Over diagnosis of typhoid and malaria co-infection by health care workers in north central Nigeria: A cross-sectional study," Nigerian Journal of Medicine, vol. 29, no. 1, pp. 100–103, 2020. DOI: https://doi.org/10.4103/1115-2613.284868.

[3] World Health Organization, World Malaria Report 2023. Geneva, Switzerland: World Health Organization, 2023. ISBN: 978-92-4-008617-3.

[4] World Health Organization, "Typhoid," Mar. 30, 2023. Available: https://www.who.int/news-room/fact-sheets/detail/typhoid.

[5] C. M. Parry, I. Ribeiro, K. Walia, P. Rupali, S. Baker, and B. Basnyat, "Multidrug resistant enteric fever in South Asia: Unmet medical needs and opportunities," BMJ, vol. 364, Art. no. k5322, 2019. DOI: https://doi.org/10.1136/bmj.k5322.

[6] I. A. Simon-Oke and M. O. Akinbote, "Prevalence of malaria and typhoid coinfection in relation to haematological profile of university students in Akure, Nigeria," Journal of Infectious Diseases and Epidemiology, vol. 6, Art. no. 166, 2020. DOI: https://doi.org/10.23937/2474-3658/1510166.

[7] O. C. Collins and K. J. Duffy, "A mathematical model for the dynamics and control of malaria in Nigeria," Infectious Disease Modelling, 2022. DOI: https://doi.org/10.1016/j.idm.2022.10.005.

[8] H. W. Hethcote, “The mathematics of infectious diseases,” SIAM Review, vol. 42, no. 4, pp. 599–653, 2000. DOI: https://doi.org/10.1137/S0036144500371907.

[9] C. Vargas-De-León, “Global analysis of a delayed vector-bias model for malaria transmission with incubation period in mosquitoes,” Mathematical Biosciences and Engineering, vol. 9, no. 1, pp. 165–174, 2012. DOI: https://doi.org/10.3934/mbe.2012.9.165.

[10] A. Abdulfatai, A. AtteMomoh, I. M. Ali, B. David, and D. J. Washachi, “Mathematical modelling of malaria and typhoid co-infection incorporating vector and loss of immunity,” FUW Trends in Science & Technology Journal, 2021. Available: https://www.ftstjournal.com/uploads/docs/63%20Article%2025.pdf.

[11] O. C. Collins and O. A. Olanrewaju, “Mathematical model analysis for the dynamics and control of malaria and typhoid fever co-infection,” AppliedMath, vol. 6, no. 9, Art. no. 154, 2026. DOI: https://doi.org/10.3390/appliedmath6090154.

[12] A. I. O. Ofomata, C. O. Agwu, S. O. Adeyemo, and C. B. Okereke, “Mathematical model of drug-resistant malaria and typhoid fever co-infection with optimal control and cost effectiveness analysis,” EPRA International Journal of Research & Development, vol. 10, no. 8, 2025. DOI: https://doi.org/10.36713/epra22951.

[13] Z. A. Workie and P. R. Koya, “Mathematical modelling of the co-infection dynamics of typhoid fever with Plasmodium vivax and Plasmodium falciparum with treatment,” Mathematical Modelling and Applications, vol. 7, no. 1, pp. 1–25, 2022. DOI: https://doi.org/10.11648/j.mma.20220701.11.

[14] T. J. Oluwafemi, E. Azuaba, D. Bako, and J. Dayap, “Global stability and sensitivity analysis of malaria, dengue and typhoid triple infection,” Journal of Applied Sciences and Environmental Management, vol. 28, no. 2, pp. 543–549, 2024. DOI: https://doi.org/10.4314/jasem.v28i2.27.

[15] L. Matsebula and F. Nyabadza, “Mathematical analysis of cholera–typhoid co-infection transmission dynamics,” Frontiers in Applied Mathematics and Statistics, vol. 8, Art. no. 892098, pp. 1–13, 2022. DOI: https://doi.org/10.3389/fams.2022.892098.

[16] I. A. Olopade, T. O. Akinwumi, S. O. Ajao, I. T. Mohammed, S. O. Sangoniyi, G. A. Adeniran, B. O. Bello, and S. O. Adewale, “Analyzing the mathematical impact of vaccination in mitigating Rift Valley fever spread among livestock,” African Journal of Sciences and Traditional Medicine, vol. 1, no. 1, pp. 43–68, 2024. DOI: https://doi.org/10.58578/ajstm.v1i1.3361.

[17] I. Olopade, S. Ajao, T. Akinwumi, G. Adeniran, R. Aderenle, and A. Adesanya, "Mathematical modelling of the impacts of syphilis multi-stage treatments," Modeling Earth Systems and Environment, vol. 4, pp. 5489–5502, 2024.

[18] M. K. Savi, "An overview of malaria transmission mechanisms, control, and modeling," Medical Sciences, vol. 11, no. 1, Art. no. 3, 2022. DOI: https://doi.org/10.3390/medsci11010003.

[19] J. A. Crump, "Progress in typhoid fever epidemiology," Clinical Infectious Diseases, vol. 68, suppl. 1, pp. S4–S9, 2019. DOI: https://doi.org/10.1093/cid/ciy846.

[20] S. Mandal, R. R. Sarkar, and S. Sinha, "Mathematical models of malaria: A review," Malaria Journal, vol. 10, Art. no. 202, 2011. DOI: https://doi.org/10.1186/1475-2875-10-202.

[21] T. S. Churcher, R. E. Sinden, N. J. Edwards, I. D. Poulton, T. W. Rampling, P. M. Brock, J. T. Griffin, L. M. Upton, S. E. Zakutansky, K. A. Sala, F. Angrisano, A. V. Hill, and A. M. Blagborough, "Probability of transmission of malaria from mosquito to human is regulated by mosquito parasite density in naïve and vaccinated hosts," PLOS Pathogens, vol. 13, no. 1, Art. no. e1006108, 2017. DOI: https://doi.org/10.1371/journal.ppat.1006108.

[22] J. S. Gunn, J. M. Marshall, S. Baker, S. Dongol, R. C. Charles, and E. T. Ryan, "Salmonella chronic carriage: Epidemiology, diagnosis, and gallbladder persistence," Trends in Microbiology, vol. 22, no. 11, pp. 648–655, 2014. DOI: https://doi.org/10.1016/j.tim.2014.06.007.

[23] I. A. Olopade, E. I. Akinola, M. E. Philemon, I. T. Mohammed, S. O. Ajao, S. O. Sangoniyi, and G. A. Adeniran, "Modeling the mathematical transmission of a pneumonia epidemic model with awareness," Journal of Applied Sciences and Environmental Management, vol. 28, no. 2, pp. 403–413, 2024.

[24] I. A. Olopade, A. O. Adesanya, I. T. Mohammed, M. A. Afolabi, and A. O. Oladapo, "Mathematical analysis of the global dynamics of an SVEIR epidemic model with herd immunity," International Journal of Science and Engineering Investigations, vol. 6, no. 69, pp. 141–148, 2017. Available: http://www.ijsei.com/ins.htm.

[25] S. T. Tresna, Subiyanto, and S. Supian, "Mathematical models for typhoid disease transmission: A systematic literature review," Mathematics, vol. 10, no. 14, Art. no. 2506, 2022. DOI: https://doi.org/10.3390/math10142506.

[26] P. Wilairatana, W. Mala, W. K. Klangbud, K. U. Kotepui, P. Rattaprasert, and M. Kotepui, "Prevalence, probability, and outcomes of typhoidal/non-typhoidal Salmonella and malaria co-infection among febrile patients: A systematic review and meta-analysis," Scientific Reports, vol. 11, no. 1, Art. no. 21889, 2021. DOI: https://doi.org/10.1038/s41598-021-01443-y.

[27] P. Wilairatana, W. Mala, F. R. Masangkay, K. U. Kotepui, and M. Kotepui, "The prevalence of malaria and bacteremia co-infections among febrile patients: A systematic review and meta-analysis," Tropical Medicine and Infectious Disease, vol. 7, no. 9, Art. no. 243, 2022. DOI: https://doi.org/10.3390/tropicalmed7090243.

[28] O. Akinola, "Dispelling the malaria–typhoid co-infection myth in Nigeria: A literature review," International Journal of Sciences: Basic and Applied Research, vol. 72, no. 1, pp. 145–156, 2024.

[29] M. S. Alhaj, "Mathematical model for malaria disease transmission," Journal of Mathematical Analysis and Modeling, vol. 4, no. 1, pp. 1–16, 2023. DOI: https://doi.org/10.48185/jmam.v4i1.664.

[30] S. Y. Tchoumi, H. Rwezaura, and J. M. Tchuenche, "A mathematical model with numerical simulations for malaria transmission dynamics with differential susceptibility and partial immunity," Healthcare Analytics, vol. 3, Art. no. 100165, 2023. DOI: https://doi.org/10.1016/j.health.2023.100165.

[31] P. Duve, S. Charles, J. Munyakazi, R. Lühken, and P. Witbooi, "A mathematical model for malaria disease dynamics with vaccination and infected immigrants," Mathematical Biosciences and Engineering, vol. 21, no. 1, pp. 1082–1109, 2024. DOI: https://doi.org/10.3934/mbe.2024047.

[32] F. O. Ochieng, "SEIRS model for malaria transmission dynamics incorporating seasonality and awareness campaign," Infectious Disease Modelling, vol. 9, no. 1, pp. 84–102, 2024. DOI: https://doi.org/10.1016/j.idm.2023.12.002.

[33] B. Agbata, J. Amoah-Mensah, P. Kwabi, Q. Ahman, F. Asantemensa, and W. Obeng-Denteh, "Mathematical modelling and analysis of malaria model with effects of vaccination and treatment intervention," Journal of Pharmaceutical & Allied Sciences, vol. 22, no. 2, 2025.

[34] E. Akowe, Q. O. Ahman, B. C. Agbata, S. O. Joseph, E. O. Senewo, A. Y. Danjuma, and D. J. Yahaya, "A novel malaria mathematical model: Integrating vector and non-vector transmission pathways," BMC Infectious Diseases, vol. 25, Art. no. 322, 2025. DOI: https://doi.org/10.1186/s12879-025-10655-y.

[35] F. K. Alalhareth, M. H. Alharbi, and M. A. Ibrahim, "Modeling typhoid fever dynamics: Stability analysis and periodic solutions in epidemic model with partial susceptibility," Mathematics, vol. 11, no. 17, Art. no. 3713, 2023. DOI: https://doi.org/10.3390/math11173713.

[36] S. K. Kailan and B. Seidu, “A mathematical model on the transmission dynamics of typhoid fever with treatment and booster vaccination,” Frontiers in Applied Mathematics and Statistics, vol. 9, Art. no. 1151270, 2023. DOI: https://doi.org/10.3389/fams.2023.1151270.

[37] F. O. Lawal, T. T. Yusuf, A. Abidemi, and O. Olotu, “A non-linear mathematical model for typhoid fever transmission dynamics with medically hygienic compartment,” Modeling Earth Systems and Environment, vol. 10, no. 5, pp. 6213–6232, 2024. DOI: https://doi.org/10.1007/s40808-024-02052-1.

[38] K. A. Tijani, C. E. Madubueze, and R. I. Gweryina, “Modelling typhoid fever transmission with treatment relapse response: Optimal control and cost-effectiveness analysis,” Mathematical Models and Computer Simulations, vol. 16, no. 3, pp. 457–485, 2024. DOI: https://doi.org/10.1134/S207004822403014X.

[39] T. J. Tsafack, C. K. Kum, A. J. O. Tassé, and B. Tsanou, “Mathematical modelling of the dynamics of typhoid fever and two modes of treatment in a health district in Cameroon,” Mathematical Biosciences and Engineering, vol. 22, no. 2, pp. 477–510, 2025. DOI: https://doi.org/10.3934/mbe.2025021.

[40] J. M. Mutua, F.-B. Wang, and N. K. Vaidya, “Modeling malaria and typhoid fever co-infection dynamics,” Mathematical Biosciences, vol. 264, pp. 128–144, 2015. DOI: https://doi.org/10.1016/j.mbs.2015.03.014.

[41] I. A. Olopade, S. O. Ajao, M. T. Idayat, S. F. Iorhen, and E. M. Philemon, “Analysis of a mathematical model of transmission dynamics of HIV/AIDS with saturated incidence rate,” Ethiopian Journal of Science and Technology, vol. 17, no. 2, pp. 123–141, 2024